nature

https://doi.org/10.1038/s41586-021-04142-6

Accelerated Article Preview

Untimely TGFβ responses in COVID-19 limit antiviral functions of NK cells

Received: 30 March 2021

Accepted: 14 October 2021

Accelerated Article Preview Published online 25 October 2021

Cite this article as: Witkowski, M. et al. Untimely TGFβ responses in COVID-19 limit antiviral functions of NK cells. *Nature* https://doi.org/10.1038/s41586-021-04142-6 (2021).

Mario Witkowski, Caroline Tizian, Marta Ferreira-Gomes, Daniela Niemeyer, Terry C. Jones, Frederik Heinrich, Stefan Frischbutter, Stefan Angermair, Thordis Hohnstein, Irene Mattiola, Philipp Nawrath, Sophie Mc Ewen, Silvia Zocche, Edoardo Viviano, Gitta Anne Heinz, Marcus Maurer, Uwe Kölsch, Robert Lorenz Chua, Tom Aschman, Christian Meisel, Josefine Radke, Birgit Sawitzki, Jobst Roehmel, Kristina Allers, Verena Moos, Thomas Schneider, Leif Hanitsch, Marcus A. Mall, Christian Conrad, Helena Radbruch, Claudia U. Duerr, Joseph A. Trapani, Emanuela Marcenaro, Tilmann Kallinich, Victor M. Corman, Florian Kurth, Leif Erik Sander, Christian Drosten, Sascha Treskatsch, Pawel Durek, Andrey Kruglov, Andreas Radbruch, Mir-Farzin Mashreghi & Andreas Diefenbach

Article

Untimely TGFβ responses in COVID-19 limit antiviral functions of NK cells

https://doi.org/10.1038/s41586-021-04142-6

Received: 30 March 2021

Accepted: 14 October 2021

Published online: 25 October 2021

Mario Witkowski[1,2,3,26]✉, Caroline Tizian[1,2,26], Marta Ferreira-Gomes[4,26], Daniela Niemeyer[5,6], Terry C. Jones[5,6,7], Frederik Heinrich[4], Stefan Frischbutter[8], Stefan Angermair[9], Thordis Hohnstein[1,2], Irene Mattiola[1,2], Philipp Nawrath[1,2], Sophie Mc Ewen[1,2], Silvia Zocche[10], Edoardo Viviano[11], Gitta Anne Heinz[4], Marcus Maurer[8], Uwe Kölsch[12], Robert Lorenz Chua[13], Tom Aschman[14], Christian Meisel[12], Josefine Radke[14], Birgit Sawitzki[15], Jobst Roehmel[16], Kristina Allers[17], Verena Moos[17], Thomas Schneider[17], Leif Hanitsch[15], Marcus A. Mall[16,18], Christian Conrad[13], Helena Radbruch[14], Claudia U. Duerr[19], Joseph A. Trapani[20], Emanuela Marcenaro[21], Tilmann Kallinich[4,18,22], Victor M. Corman[5,6], Florian Kurth[23], Leif Erik Sander[23], Christian Drosten[5,6], Sascha Treskatsch[9], Pawel Durek[4], Andrey Kruglov[4,24,25], Andreas Radbruch[4], Mir-Farzin Mashreghi[4,18,25,27] & Andreas Diefenbach[1,2,3,27]✉

SARS-CoV-2 is a single-stranded RNA virus that causes coronavirus disease 2019 (COVID-19). Given its acute and often self-limiting course, components of the innate immune system are likely central in controlling virus replication thereby determining clinical outcome. Natural killer (NK) cells are innate lymphocytes with notable activity against a broad range of viruses, including RNA viruses[1,2]. NK cell function may be altered during COVID-19 despite increased representation of NK cells with an activated and 'adaptive' phenotype[3,4]. Here we show that viral load decline in COVID-19 correlates with NK cell status and that NK cells can control SARS-CoV-2 replication by recognizing infected target cells. In severe COVID-19, NK cells show remarkable defects in virus control, cytokine production and cell-mediated cytotoxicity despite high expression of cytotoxic effector molecules. Single-cell RNA-sequencing (scRNA-seq) of NK cells along the time course of the entire COVID-19 disease spectrum reveals a unique gene expression signature. Transcriptional networks of interferon-driven NK cell activation are superimposed by a dominant TGFβ response signature with reduced expression of genes related to cell-cell adhesion, granule exocytosis and cell-mediated cytotoxicity. In severe COVID-19, serum levels of TGFβ peak during the first 2 weeks of infection, and serum obtained from these patients profoundly inhibits NK cell function in a TGFβ-dependent manner. Our data reveal that untimely production of TGFβ is a hallmark of severe COVID-19 and may inhibit NK cell function and early virus control.

[1]Laboratory of Innate Immunity, Institute of Microbiology, Infectious Diseases and Immunology, Charité - Universitätsmedizin Berlin, Corporate Member of Freie Universität Berlin, Humboldt-Universität zu Berlin, Campus Benjamin Franklin, Berlin, Germany. [2]Mucosal and Developmental Immunology, Deutsches Rheuma-Forschungszentrum (DRFZ), an Institute of the Leibniz Association, Berlin, Germany. [3]Department of Microbiology and Hygiene, Labor Berlin, Charité - Vivantes GmbH, Berlin, Germany. [4]Therapeutic Gene Regulation, Deutsches Rheuma-Forschungszentrum (DRFZ), an Institute of the Leibniz Association, Berlin, Germany. [5]Institute of Virology, Charité - Universitätsmedizin Berlin, Corporate Member of Freie Universität Berlin and Humboldt-Universität zu Berlin, Campus Charité Mitte, Berlin, Germany. [6]German Centre for Infection Research (DZIF), Associated Partner Site, Berlin, Germany. [7]Centre for Pathogen Evolution, Department of Zoology, University of Cambridge, Cambridge, UK. [8]Dermatological Allergology, Allergie-Centrum-Charité, Department of Dermatology and Allergy, Charité - Universitätsmedizin Berlin, Corporate Member of Freie Universität Berlin and Humboldt-Universität zu Berlin, Campus Charité Mitte, Berlin, Germany. [9]Department of Anesthesiology and Intensive Care Medicine, Charité - Universitätsmedizin Berlin, Corporate Member of Freie Universität Berlin and Humboldt-Universität zu Berlin, Campus Benjamin Franklin, Berlin, Germany. [10]Department of Pediatric Gastroenterology, Nephrology and Metabolic Diseases, Charité - Universitätsmedizin Berlin, Corporate Member of Freie Universität Berlin and Humboldt-Universität zu Berlin, Campus Virchow-Klinikum, Berlin, Germany. [11]Institute of Physiology, Center for Space Medicine and Extreme Environments Berlin, Charité–Universitätsmedizin Berlin, Corporate Member of Freie Universität Berlin and Humboldt-Universität zu Berlin, Berlin, Germany. [12]Institute of Medical Immunology, Charité, Universitätsmedizin Berlin, Berlin, Germany; Department of Immunology, Labor Berlin-Charité Vivantes, Berlin, Germany. [13]Center for Digital Health, Berlin Institute of Health (BIH) and Charité-Universitätsmedizin Berlin, corporate member of Freie Universität Berlin, Humboldt-Universität zu Berlin, Berlin, Germany. [14]Department of Neuropathology, Charité-Universitätsmedizin Berlin, corporate member of Freie Universität Berlin and Humboldt-Universität zu Berlin, Berlin, Germany. [15]Institute of Medical Immunology, Charité - Universitätsmedizin Berlin, Corporate Member of Freie Universität Berlin and Humboldt-Universität zu Berlin, Campus Virchow-Klinikum, Augustenburger Platz1, Berlin, Germany. [16]Department of Pediatric Respiratory Medicine, Immunology and Critical Care Medicine, Charité-Universitätsmedizin Berlin, corporate member of Freie Universität Berlin and Humboldt-Universität zu Berlin, Campus Virchow-Klinikum, Augustenburger Platz1, Berlin, Germany. [17]Department of Medicine (Gastroenterology, Infectious Diseases, Rheumatology), Charité - Universitätsmedizin Berlin, corporate member of Freie Universität Berlin, Humboldt-Universität zu Berlin and Berlin Institute of Health, Campus Benjamin Franklin, Berlin, Germany. [18]German Center for Lung Research (DZL), associated partner, Berlin, Germany. [19]Laboratory of Mucosal Immunity, Institute of Microbiology, Infectious Diseases and Immunology, Charité – Universitätsmedizin Berlin, Corporate Member of Freie Universität Berlin, Humboldt-Universität zu Berlin, Campus Benjamin Franklin, Hindenburgdamm 30, Berlin, Germany. [20]Cancer Immunology Program, Peter MacCallum Cancer Centre, Melbourne, Victoria, Australia. [21]Department of Experimental Medicine and Centre of Excellence for Biomedical Research, University of Genoa, Genoa, Italy. [22]Chronic inflammation in childhood, Deutsches Rheuma-Forschungszentrum (DRFZ), an Institute of the Leibniz Association, Berlin, Germany. [23]Department of Infectious Diseases and Respiratory Medicine, Charité - Universitätsmedizin Berlin, corporate member of Freie Universität Berlin and Humboldt-Universität zu Berlin, Berlin, Germany. [24]Belozersky Institute of Physico-Chemical Biology and Biological Faculty, M.V. Lomonosov Moscow State University, Moscow, Russia. [25]Center for Precision Genome Editing and Genetic Technologies for Biomedicine, Engelhardt Institute of Molecular Biology, Russian Academy of Sciences, Moscow, Russia. [26]These authors contributed equally: Mario Witkowski, Caroline Tizian, Marta Ferreira-Gomes. [27]These authors jointly supervised this work: Mir-Farzin Mashreghi, Andreas Diefenbach. ✉e-mail: mario.witkowski@charite.de; andreas.diefenbach@charite.de

The role of NK cells during SARS-CoV-2 infections remains unknown. We wondered if we could find differences in the SARS-CoV-2 load decline between hospitalized patients with "normal" (> 40 NK/µl) or "low" (≤ 40 NK/µl) NK cell counts. We found an overall pattern of faster decline of viral load in patients with "normal" NK cell counts (Fig. 1a,b) across patient groups with different overall clinical status (Extended Data Fig. 1a, Supplementary Table 3). Importantly, such negative correlation between cell count (early during the infection) and viral load was not found for T cells or B cells (Extended Data Fig. 1a). Similarly, a more rapid decline in viral load over time was associated with a more rapid increase in NK cells and *vice versa* (Extended Data Fig. 1b). Collectively, availability of NK cells early during COVID-19 correlated with lower abundance of SARS-CoV-2 viral RNA.

We explored if NK cells can directly control SARS-CoV-2 (B.1 lineage) replication in an infected human lung epithelial cell line (Calu-3) or in kidney epithelial cells (VERO E6). At the time of infection, highly purified NK cells from healthy donors were added and intracellular viral load was measured. NK cells dose-dependently reduced viral replication (Fig. 1c,d), a finding which was confirmed with a second virus variant (B.1.351 lineage; Extended Data Fig. 1c). NK cells are often activated during viral infections[5], but NK cells from hospitalized COVID-19 patients were significantly less effective in reducing viral load when compared to NK cells from healthy donors (Fig. 1e,f).

NK cell recognition of virus-infected cells is determined by interactions of activating and inhibitory NK cell receptors with their ligands on target cells[6]. The profound reduction of viral replication by NK cells could not be further enhanced by HLA blockade, suggesting that infected Calu-3 cells do not appreciably inhibit NK cells via HLA-I-specific inhibitory receptors (Fig. 1g). Uninfected Calu-3 cells were poor NK cell targets (Extended Data Fig. 1d). While blockade of single activating NK cell receptors did not impair virus control, simultaneous blockade of all three NCRs or of 2B4, NKG2D and DNAM-1 led to a significant increase in virus replication (Fig. 1g). Collectively, our data demonstrate that NK cell-mediated control of SARS-CoV-2 replication in infected target cells requires redundant recognition by activating NK cell receptors, a process robustly impaired when using NK cells from hospitalized patients with COVID-19.

Impaired NK cell function during COVID-19

We set out to study NK cell effector functions in detail in patients with COVID-19 across the disease spectrum and time (Fig. 2a). Patients with non-COVID-19, flu-like illness (FLI), as well as ambulant and moderate COVID-19 patients had normal frequencies of $CD56^{bright}$ and $CD56^{dim}$ NK cells, whereas those with a severe course of COVID-19 had reduced frequencies of both NK cell subsets and of type 1 ILCs already during the first week following symptom onset (Extended Data Fig. 2).

Previous data regarding the expression of cytotoxic molecules was inconclusive[3,4,7,8]. We found a significant and early up-regulation of perforin and granzyme B both in ambulant and hospitalized COVID-19 patients (Fig. 2b,c; Extended Data Fig. 3a-c), an early sign of NK cell activation observed in the context of various other viral infections[5,9–11]. Surprisingly, NK cells isolated during the first week after symptom onset from hospitalized and, to a lesser extent, also from ambulant COVID-19 patients were impaired in cell-mediated cytotoxicity despite their high-level perforin and granzyme B expression (Fig. 2d). Such reduced cytotoxic activity of NK cells was not found in FLI patients. Given the apparent paradox of high-level expression of cytotoxic molecules and low cytotoxic function, we analyzed the release of cytotoxic granules. While NK cells from healthy controls, FLI and ambulant COVID-19 patients showed no robust differences, NK cells from hospitalized COVID-19 patients were impaired in degranulation (Fig. 2e, Extended Data Fig. 3d). One of the first steps during cognate NK cell-target cell interactions is the formation of cellular conjugates, establishment of which was reduced when using NK cells from severe COVID-19 patients (Fig. 2f,g). Reduced cell-cell interactions and degranulation were not a consequence of reduced expression of activating NK cell receptors in severe COVID-19 (Extended Data Fig. 3e,f).

While NK cells from ambulant COVID-19 patients showed increased production of IFNγ, NK cells from severe COVID-19 patients produced only very low levels of IFNγ and TNF (Extended Data Fig. 3g,h)[12]. The T-box transcription factor T-bet coordinates NK cell effector programs, including the expression of granzyme B, perforin and IFNγ[13]. T-bet was upregulated in NK cells from patients with FLI and its expression was maintained in ambulant COVID-19 patients, but it was substantially suppressed at all timepoints in NK cells from hospitalized COVID-19 patients (Extended Data Fig. 3a,i). These data cannot be easily explained by differences of age, because we did not find any strong negative correlation between age and any of the NK cell readouts (Extended Data Fig. 4). Reductions in NK cell-mediated cytotoxicity and effector programs were also not caused by dexamethasone treatment, as comparable data were obtained during the first COVID-19 wave (March/April 2020) when dexamethasone was not administered (Fig. 2e).

scRNA-seq atlas of NK cells from COVID-19

We generated a time-resolved, droplet-based single-cell transcriptomic atlas of peripheral blood NK cells of patients with severe COVID-19, outpatients with oligosymptomatic SARS-CoV-2 infection and of healthy donors (Fig. 3a). Using the gating strategy depicted in Extended Data Fig. 5a, a total of 80,325 single NK cell transcriptomes were captured. Employing *Uniform Manifold Approximation and Projection for Dimension Reduction* (UMAP), we identified 7 transcriptionally distinct clusters of cells (Fig. 3a)[14]. A small number (1,375 cells) of contaminating non-NK cells was found in cluster 6, which was excluded from further analysis. Cells in the remaining clusters 0-5 expressed genes that define conventional NK cells, including surface markers (Extended Data Fig. 5b), effector molecules, such as *PRF1*, *GNLY*, *GZMB, GZMH* and *GZMM*, and *TBX21* (encoding T-bet) (Extended Data Fig. 5b-f)[15,16]. Cluster 2 represented $CD56^{bright}$ NK cells characterized by high expression of *IL7R*, *SELL*, *XCL1*, *LTB*, *GZMK* and low expression of *CD160* (Extended Data Fig. 5b,c)[16,17]. Cluster 0 contained cells with high expression of NK cell effector molecules and of *TBX21* but with lower expression of *NCAM1*, which we therefore identified as a subset of $CD56^{dim}$ NK cells. Cluster 1 was closely related to cluster 0. Among the few differentially expressed genes were *CD96* and *KLRG1*, both of which have been linked to NK cell maturation and functional exhaustion[18,19]. In addition, they showed reduced expression of most NK effector genes, thus demarcating late effector NK cells that may be reduced in function (Extended Data Fig. 5f). Within $CD56^{dim}$ NK cells, a third cluster (cluster 3) was discriminated with low expression of effector molecules (*GZMB, GZMH*, *GZMM*; Extended Data Fig. 5d). This NK cell subset may correspond to the previously described "terminally differentiated" $CD56^{dim}$ NK cells that are in a post-activation state[16,20].

Similar to $CD56^{bright}$ NK cells, cells in cluster 4 were characterized by high expression of *IL7R* and *GZMK* but expressed lower levels of *XCL1* and *SELL* (Extended Data Fig. 5c), corresponding to "transitional NK cells"[16]. Cluster 4 also contained cells expressing the activating NK cell receptor *KLRC2* (encoding NKG2C; Extended Data Fig. 5e). Low expression levels of NKG2A (*KLRC1*) and of the signaling adaptor molecule FcεRγ (*FCER1G*) corroborate the enrichment of adaptive NK cells in cluster 4[21]. Thus, cluster 4 is heterogenous representing transitional and adaptive NK cells. Cluster 5 represented proliferating NK cells identified by high expression of *MIK67* and of genes controlling cell cycle (Extended Data Figure 5e,g).

Analysis of the representation of each NK cell cluster across COVID-19 disease states revealed dynamics in NK cell differentiation. In severe COVID-19, we observed a significant increase of proliferating (cluster 5) NK cells (Fig. 3b), in line with flow cytometry data (Extended Data Fig. 5h). While the frequency of cells belonging to cluster 1 (late effector)

NK cells was reduced in patients with severe COVID-19, these patients had an increase of "terminally differentiated" cluster 3 NK cells (Fig. 3b). Although not statistically significant, adaptive NK cells (cluster 4) were reproducibly increased in severe COVID-19, in line with previous data[3].

To investigate if COVID-19 introduces changes in the dynamics of NK cell differentiation, we employed *Monocle Pseudotime Trajectory Analysis*[22], which connects related clusters to construct differentiation trajectories (Fig. 3c,d, Extended Data Fig. 6a-d). We defined cluster 2 CD56^{bright} NK cells as the root of the progression trajectory. The pseudotime model predicts that CD56^{bright} NK cells (cluster 2), via a proliferative state in the left leaf (cluster 5), differentiate into effector NK cells (cluster 0: CD56^{dim} NK effector I) and, by gradually decreasing effector molecule expression, into cluster 1 CD56^{dim} effector II cells until reaching the terminally differentiated state (cluster 3) dominating the distal right leaf of the differentiation trajectory (Fig. 3c,d, Extended Data Fig. 6a,b). Along the pseudotime trajectory, major differentiation states were CD56^{bright} NK cells (state 12: high expression of *IL7RA* and *GZMK*), proliferating NK cells (state 1: *MKI67* high), effector NK cells (state 2-7) with graded levels of effector genes such as *PRF1* and lastly terminally-differentiated NK cells (state 8, 9; Extended Data Fig. 6c,d). This differentiation trajectory was generally conserved in COVID-19 patients, but particularly severe COVID-19 patients had a marked increase in proliferating NK cells which fed into one root of the differentiation trajectory and an accumulation of terminally-differentiated NK cells at the distal end of the trajectory (Extended Data Fig. 6a-d).

TGFβ signature is a hallmark of severe COVID-19

We interrogated our dataset for enrichment of genes that may affect NK cell effector functions. By applying gene set enrichment analysis (GSEA) to the effector NK cell clusters 0, 1 and 3, we observed in patients with COVID-19 a significant enrichment of "Hallmark IFNα response genes" (Fig. 3e) and of "Hallmark IFNγ response genes" (Extended Data Fig. 6e) predominantly in the NK effector cluster 0, in line with increased virus-induced type I and type II interferons in the serum of COVID-19 patients (Extended Data Fig. 6f). We also confirmed[3] increased expression of markers linked to NK cell activation and differentiation (e.g., CD69 and CD57) in hospitalized patients (Extended Data Fig. 6g-i). Among the enriched functional networks in NK cells from COVID-19 patients were several gene sets related to cellular metabolism and translation, demonstrating profound changes in cellular activation in the context of SARS-CoV-2 infections (Extended Data Fig. 7a).

We noted that among the transcriptional networks significantly enriched in effector NK cells of ambulant and, more robustly, of severe COVID-19 cases, was the KEGG pathway "Intestinal Immune Network for IgA Production" (Extended Data Fig. 7b). IgA class switch is strictly controlled by TGFβ[23,24] and many genes in this KEGG pathway are direct targets of TGFβ signaling, a cytokine well known to suppress NK cell function[25,26]. Even terminally differentiated (cluster 3) NK cells, profoundly depleted in gene sets regulated by IFNα or cellular metabolism (Extended Data Fig. 7a), were enriched for genes of this KEGG pathway (Extended Data Fig. 7b). Because the transcriptional changes instructed by TGFβ in NK cells are not known at single cell resolution, we generated a scRNA-seq dataset of highly purified peripheral blood NK cells of healthy donors cultured in the presence or absence of TGFβ. UMAP analysis of the two treatment groups showed a profound effect of TGFβ on the transcriptional state of NK cells which was highly reproducible across individual donors (Extended Data Fig. 8a). Analysis of differentially expressed genes revealed that the majority of genes were negatively regulated by TGFβ in their expression, including *TBX21* and *STAT1* but also a number of effector genes, such as *PRF1* and granzyme family members (Extended Data Fig. 8b). A smaller group of genes was induced in expression by exposure to TGFβ, among them, genes encoding for the chemokine receptor CXCR4 or for the transcription factor EOMES, both known TGFβ-target genes (Extended Data Fig. 8b). Within the cells that were exposed to TGFβ (Extended Data Fig. 8c, red), we found various pathways central to granule exocytosis[27] to be negatively regulated by TGFβ (Extended Data Fig. 8d).

Using the TGFβ signature established above, we interrogated our scRNA-seq dataset from COVID-19 patients for changes in the expression of TGFβ-controlled genes. TGFβ-controlled genes were expressed at a low level in NK cells from healthy donors, but a robust enrichment of TGFβ response genes was noted particularly in effector NK cell clusters during severe COVID-19 (Fig. 3f). Importantly, changes in the expression of TGFβ-controlled genes were already detectable during the very early stages of COVID-19 and increased during the course of infection (Fig. 3g). Indeed, the expression of canonical TGFβ target genes such as *EOMES* and *ITGAE* was upregulated in NK cells of severe COVID-19 patients (Extended Data Fig. 8e,f). Our data demonstrate a progressive and long-lasting reprogramming of NK cells by TGFβ during COVID-19 starting within the first days after symptom onset and commensurate with disease severity.

In ambulant COVID-19, gene sets associated with cell adhesion and NK cell cytotoxicity were mildly upregulated in some NK cells. However, substantial downregulation was found in a majority of effector NK cells in severe COVID-19 (Extended Data Fig. 8g). Interestingly, among the genes profoundly downregulated in severe COVID-19 patients was *ITGB2*, encoding β2 integrin (CD18), which associates with the α integrins CD11a-d to generate functional integrin receptors (Extended Data Fig. 8h) and is involved in NK cell-mediated cytotoxicity[28,29]. This may provide a molecular explanation for the profound failure of NK cells from severe COVID-19 to form conjugates with target cells. Collectively, NK cells from severe COVID-19 show a gene signature characterized by IFN-controlled cell activation programs (e.g., upregulation of perforin, granzyme B and CD69) superimposed by profound and long-lasting TGFβ-controlled transcriptional reprogramming, in particular the downregulation of genes linked to NK cell-mediated cytotoxicity.

We wondered whether re-programming of NK cells by TGFβ is a common event in pneumonia. We extracted NK cells from previously published scRNA-seq dataset of PBMC from patients with COVID-19 and influenza pneumonia[30] and observed a strong enrichment of TGFβ-controlled genes in NK cells from COVID-19 but not from influenza pneumonia (Fig. 3h). To explore whether TGFβ signatures can also be found in lung NK cells, we analyzed a single nucleus RNA-seq dataset from post-mortem lung tissue of patients with severe COVID-19 or with SARS-CoV-2-negative pneumonia[31]. The dataset allowed for the analysis of single-cell transcriptomes of lung NK cells (Extended Data Fig. 9a-c). GSEA analysis revealed that lung NK cells from severe COVID-19 pneumonia but not those from SARS-CoV-2-negative pneumonia were significantly enriched in TGFβ-controlled genes (Extended Data Fig. 9d).

Untimely peak of serum TGFβ in severe COVID-19

Our transcriptional and functional data suggested production of TGFβ during the early phase of SARS-CoV-2 infection, particularly in the context of severe COVID-19. While FLI and ambulant COVID-19 patients did not show increased serum TGFβ within the first week after symptom onset, hospitalized patients had significantly increased TGFβ serum levels at week 1 which peaked at week 2 (Fig. 4a). Ambulant patients showed only a smaller increment in serum TGFβ at later timepoints of the infection (>3 weeks after symptom onset). To obtain insights into the cellular sources of TGFβ, we analyzed the lung single-nuclei RNA-seq dataset for *TGFB* transcripts and for transcripts associated with TGFβ bioactivity. In comparison to non-COVID-19 pneumonias, we observed a robust increase in *TGFB1* and *TGFB2* expression in type 1 alveolar epithelial cells, fibroblasts, myofibroblasts, endothelial cells and myeloid cells (Extended Data Fig. 9e,g). Expression of various genes required for the bioactivity of TGFβ (such as *LTBP3, LAP3* and *MMP2*) were also increased in COVID-19 patients (Extended Data

Fig. 9f). Interestingly, some of the clusters with the highest expression of *TGFB1*, *LAP3* and *MMP28* contained SARS-CoV-2 transcripts (i.e., were infected) (Extended Data Fig. 9h). Thus, the early TGFβ peak in hospitalized COVID-19 patients is closely correlated with the early impairment of NK cell effector programs.

We wondered whether exposure of NK cells to TGFβ has any effect on their capacity to control viral replication. Strikingly, TGFβ completely abrogated the NK cell effector program: NK cell-mediated control of SARS-CoV-2 replication *in vitro* (Fig. 4b), cell-mediated cytotoxicity, degranulation in response to target cells and cytokine production (Extended Data Fig. 10a-d). TGFβ treatment of stimulated NK cells also led to profound downregulation of T-bet, whereas the canonical TGFβ target EOMES was upregulated (Extended Data Fig. 10e,f).

Exposure of NK cells from healthy donors to serum from severe COVID-19 patients, obtained during the first weeks after symptom onset, significantly inhibited NK cell degranulation and T-bet expression (Fig. 4c,d). This inhibitory effect was lost, when sera had been pre-treated with a TGFβ-blocking antibody with activity against TGFβ1, 2 and 3 (Fig. 4e,f; Extended Data Fig. 10g-i). In contrast, neutralization of IL-6, IL-10 or IL-15 did not restore NK cell degranulation or T-bet expression (Extended Data Fig. 10j-p) although these cytokines have been previously linked to severe COVID-19[4,32]. Thus, untimely TGFβ expression leads to suppressed NK cell function which may reduce virus control and may be a determinant severe COVID-19.

While TGFβ is widely believed to curtail excessive immune responsiveness and restore or maintain immune homeostasis[33], we now demonstrate that untimely early TGFβ expression and associated NK cell dysfunction is a hallmark of severe COVID-19. Multilevel proteomics data support a specific dysregulation of TGFβ signaling by SARS-CoV-2 ORF8[34] and we had previously shown that TGFβ impairs B cell responses in the context of COVID-19 (ref. [35]). Two MMP inhibitors (prinimostat, marimastat) that diminish TGFβ bioactivity profoundly inhibited replication of SARS-CoV-2 but not of SARS-CoV[34]. TGFβ-mediated impairment of NK cell function may also have an impact on other aspects of COVID-19. A dysregulated myeloid response is another hallmark of severe COVID-19 with inadequate production of inflammatory cytokines[36,37]. Lessons learned from genetic syndromes of NK cell cytotoxic defects have implicated NK cells in the quality control of innate immune responses by curtailing overzealous myeloid responses, thereby preventing immunopathology[27,38]. Another intriguing link is the role of NK cells in controlling fibrotic reprogramming and eliminating pre-fibrotic cells that undergo a senescence program[39]. Thus, inhibition of untimely TGFβ production and boosting of NK cell function may positively affect SARS-CoV-2 control on various levels.

Online content

Any methods, additional references, Nature Research reporting summaries, source data, extended data, supplementary information, acknowledgements, peer review information; details of author contributions and competing interests; and statements of data and code availability are available at https://doi.org/10.1038/s41586-021-04142-6.

1. Diaz-Salazar, C. & Sun, J. C. Natural killer cell responses to emerging viruses of zoonotic origin. *Curr Opin Virol* **44**, 97-111, https://doi.org/10.1016/j.coviro.2020.07.003 (2020).
2. Vivier, E., Tomasello, E., Baratin, M., Walzer, T. & Ugolini, S. Functions of natural killer cells. *Nat Immunol* **9**, 503-510, https://doi.org/10.1038/ni1582 (2008).
3. Maucourant, C. et al. Natural killer cell immunotypes related to COVID-19 disease severity. *Sci Immunol* **5**, https://doi.org/10.1126/sciimmunol.abd6832 (2020).
4. Mazzoni, A. et al. Impaired immune cell cytotoxicity in severe COVID-19 is IL-6 dependent. *J Clin Invest* **130**, 4694-4703, https://doi.org/10.1172/JCI138554 (2020).
5. Lucas, M., Schachterle, W., Oberle, K., Aichele, P. & Diefenbach, A. Dendritic cells prime natural killer cells by trans-presenting interleukin 15. *Immunity* **26**, 503-517 (2007).
6. Diefenbach, A. & Raulet, D. H. Innate immune recognition by stimulatory immunoreceptors. *Curr Opin Immunol* **15**, 37-44 (2003).
7. Zenarruzabeitia, O. et al. T Cell Activation, Highly Armed Cytotoxic Cells and a Shift in Monocytes CD300 Receptors Expression Is Characteristic of Patients With Severe COVID-19. *Front Immunol* **12**, 655934, https://doi.org/10.3389/fimmu.2021.655934 (2021).
8. Zheng, M. et al. Functional exhaustion of antiviral lymphocytes in COVID-19 patients. *Cell Mol Immunol* **17**, 533-535, https://doi.org/10.1038/s41423-020-0402-2 (2020).
9. Shellam, G., Allan, J., Papadimitriou, J. & Bancroft, G. Increased susceptibility to cytomegalovirus infection in beige mutant mice. *Proc. Natl. Acad. Sci. USA* **78**, 5104-5108 (1981).
10. Trinchieri, G. Biology of natural killer cells. *Adv. Immunol.* **47**, 187-376 (1989).
11. Fehniger, T. A. et al. Acquisition of Murine NK Cell Cytotoxicity Requires the Translation of a Pre-existing Pool of Granzyme B and Perforin mRNAs. *Immunity* **26**, 798-811 (2007).
12. Varchetta, S. et al. Unique immunological profile in patients with COVID-19. *Cell Mol Immunol* **18**, 604-612, https://doi.org/10.1038/s41423-020-00557-9 (2021).
13. Townsend, M. J. et al. T-bet regulates the terminal maturation and homeostasis of NK and Valpha14i NKT cells. *Immunity* **20**, 477-494 (2004).
14. Becht, E. et al. Dimensionality reduction for visualizing single-cell data using UMAP. *Nat Biotechnol*, https://doi.org/10.1038/nbt.4314 (2018).
15. Freud, A. G. et al. NKp80 Defines a Critical Step during Human Natural Killer Cell Development. *Cell Rep* **16**, 379-391, https://doi.org/10.1016/j.celrep.2016.05.095 (2016).
16. Yang, C. et al. Heterogeneity of human bone marrow and blood natural killer cells defined by single-cell transcriptome. *Nat Commun* **10**, 3931, https://doi.org/10.1038/s41467-019-11947-7 (2019).
17. Luetke-Eversloh, M., Killig, M. & Romagnani, C. Signatures of human NK cell development and terminal differentiation. *Front Immunol* **4**, 499, https://doi.org/10.3389/fimmu.2013.00499 (2013).
18. Huntington, N. D. et al. NK cell maturation and peripheral homeostasis is associated with KLRG1 up-regulation. *Journal of immunology* **178**, 4764-4770 (2007).
19. Sun, H. et al. Human CD96 Correlates to Natural Killer Cell Exhaustion and Predicts the Prognosis of Human Hepatocellular Carcinoma. *Hepatology* **70**, 168-183, https://doi.org/10.1002/hep.30347 (2019).
20. Crinier, A. et al. High-Dimensional Single-Cell Analysis Identifies Organ-Specific Signatures and Conserved NK Cell Subsets in Humans and Mice. *Immunity* **49**, 971-986 e975, https://doi.org/10.1016/j.immuni.2018.09.009 (2018).
21. Hammer, Q. et al. Peptide-specific recognition of human cytomegalovirus strains controls adaptive natural killer cells. *Nat Immunol* **19**, 453-463, https://doi.org/10.1038/s41590-018-0082-6 (2018).
22. Qiu, X. et al. Reversed graph embedding resolves complex single-cell trajectories. *Nat Methods* **14**, 979-982, https://doi.org/10.1038/nmeth.4402 (2017).
23. Coffman, R. L., Lebman, D. A. & Shrader, B. Transforming growth factor beta specifically enhances IgA production by lipopolysaccharide-stimulated murine B lymphocytes. *J Exp Med* **170**, 1039-1044, https://doi.org/10.1084/jem.170.3.1039 (1989).
24. Sonoda, E. et al. Transforming growth factor beta induces IgA production and acts additively with interleukin 5 for IgA production. *J Exp Med* **170**, 1415-1420, https://doi.org/10.1084/jem.170.4.1415 (1989).
25. Viel, S. et al. TGF-beta inhibits the activation and functions of NK cells by repressing the mTOR pathway. *Sci Signal* **9**, ra19, https://doi.org/10.1126/scisignal.aad1884 (2016).
26. Rook, A. H. et al. Effects of transforming growth factor beta on the functions of natural killer cells: depressed cytolytic activity and blunting of interferon responsiveness. *J Immunol* **136**, 3916-3920 (1986).
27. Pachlopnik Schmid, J. et al. Inherited defects in lymphocyte cytotoxic activity. *Immunol Rev* **235**, 10-23, https://doi.org/10.1111/j.0105-2896.2010.00890.x (2010).
28. Kohl, S., Springer, T. A., Schmalstieg, F. C., Loo, L. S. & Anderson, D. C. Defective natural killer cytotoxicity and polymorphonuclear leukocyte antibody-dependent cellular cytotoxicity in patients with LFA-1/OKM-1 deficiency. *J Immunol* **133**, 2972-2978 (1984).
29. Riteau, B., Barber, D. F. & Long, E. O. Vav1 phosphorylation is induced by beta2 integrin engagement on natural killer cells upstream of actin cytoskeleton and lipid raft reorganization. *J Exp Med* **198**, 469-474, https://doi.org/10.1084/jem.20021995 (2003).
30. Lee, J. S. et al. Immunophenotyping of COVID-19 and influenza highlights the role of type I interferons in development of severe COVID-19. *Sci Immunol* **5**, https://doi.org/10.1126/sciimmunol.abd1554 (2020).
31. Gassen, N. C. et al. SARS-CoV-2-mediated dysregulation of metabolism and autophagy uncovers host-targeting antivirals. *Nat Commun* **12**, 3818, https://doi.org/10.1038/s41467-021-24007-w (2021).
32. Liu, C. et al. Time-resolved systems immunology reveals a late juncture linked to fatal COVID-19. *Cell* **184**, 1836-1857 e1822, https://doi.org/10.1016/j.cell.2021.02.018 (2021).
33. Travis, M. A. & Sheppard, D. TGF-beta activation and function in immunity. *Annu Rev Immunol* **32**, 51-82, https://doi.org/10.1146/annurev-immunol-032713-120257 (2014).
34. Stukalov, A. et al. Multilevel proteomics reveals host perturbations by SARS-CoV-2 and SARS-CoV. *Nature* **594**, 246-252, https://doi.org/10.1038/s41586-021-03493-4 (2021).
35. Ferreira-Gomes, M. et al. SARS-CoV-2 in severe COVID-19 induces a TGF-β-dominated chronic immune response that does not target itself. *Nat Comm*, https://doi.org/10.1038/s41467-021-22210-3 (2021).
36. Schulte-Schrepping, J. et al. Severe COVID-19 Is Marked by a Dysregulated Myeloid Cell Compartment. *Cell* **182**, 1419-1440 e1423, https://doi.org/10.1016/j.cell.2020.08.001 (2020).
37. Merad, M. & Martin, J. C. Pathological inflammation in patients with COVID-19: a key role for monocytes and macrophages. *Nat Rev Immunol* **20**, 355-362, https://doi.org/10.1038/s41577-020-0331-4 (2020).
38. van Dommelen, S. L. et al. Perforin and granzymes have distinct roles in defensive immunity and immunopathology. *Immunity* **25**, 835-848 (2006).
39. Krizhanovsky, V. et al. Senescence of activated stellate cells limits liver fibrosis. *Cell* **134**, 657-667 (2008).

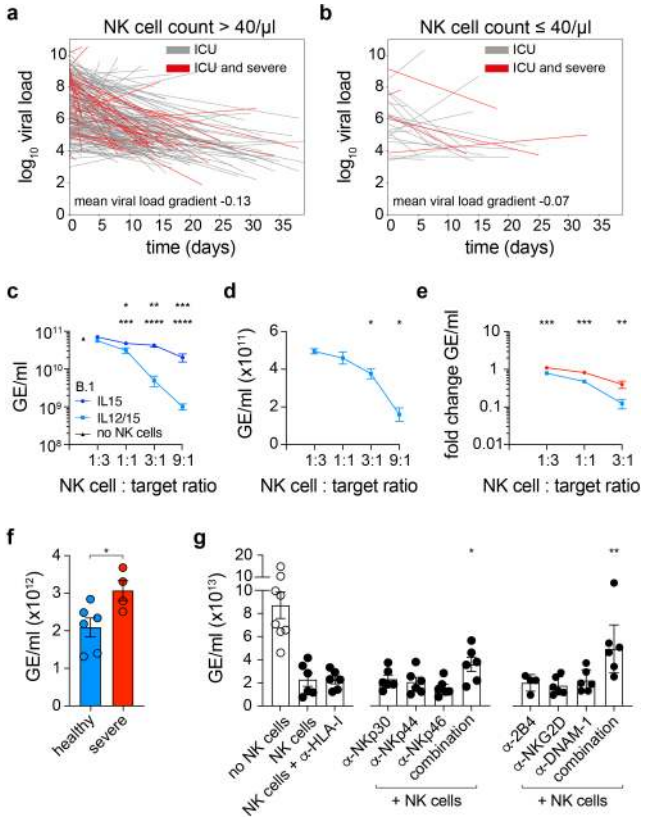

Fig. 1 | NK cells from severe COVID-19 fail to control SARS-CoV-2 replication. (**a**,**b**) Temporal viral load regression for patients with > (**a**, n=183) or ≤ (**b**, n=23) 40 NK cells/µl at first count (Methods). X-axis time in days since the first measurement. Analysis performed on 206 ICU patients (Extended Data Fig. 1) including 47 severe COVID-19 patients (highlighted in red; Supplementary Table 3). (**c**,**d**) Vero E6 cells (**c**) or Calu-3 cells (**d**) were infected with SARS-CoV-2. At 1h post infection (p.i.), NK cells from healthy donors activated for 24h *in vitro* as indicated were added. Viral replication was measured 12h later as genome equivalents (GE)/ml (target cells co-cultured with NK cells *vs.* cultured alone (c) or *vs.* E:T 1:3 (d), n=4 donors, no NK cells n=5 samples). (**e**,**f**) Vero E6 cells (**e**) or Calu-3 cells (**f**) were infected with SARS-CoV-2 and co-cultured with NK cells as described above from either healthy donors (e n=8, f n=6) or patients with severe COVID-19 (e n=6, f n=4). Viral load as fold change of Vero E6 cells cultured alone *vs.* co-cultured with NK cells was determined (**e**; pooled data from two independent experiments). For (**f**) a 1:1 NK:target cell ratio was used. (**g**) Calu-3 cells were infected and co-cultured as above with IL-12/15-activated NK cells in a 3:1 NK:target cell ratio. Prior co-culture NK cells were incubated with the indicated neutralizing receptor antibodies. Each filled dot represents viral replication of target cells co-cultured with NK cells from an individual donor (2B4 n=4, all others n=6, no NK cells n=8 samples). Graphs display mean ± SEM. Two-sided Mann-Whitney U test (indicated group *vs.* NK cell only, f; p= 0.038, g; p= 0.041and p=0.0043) (* p ≤ 0.05, ** p ≤ 0.01, *** p ≤ 0.001, **** p ≤ 0.0001).

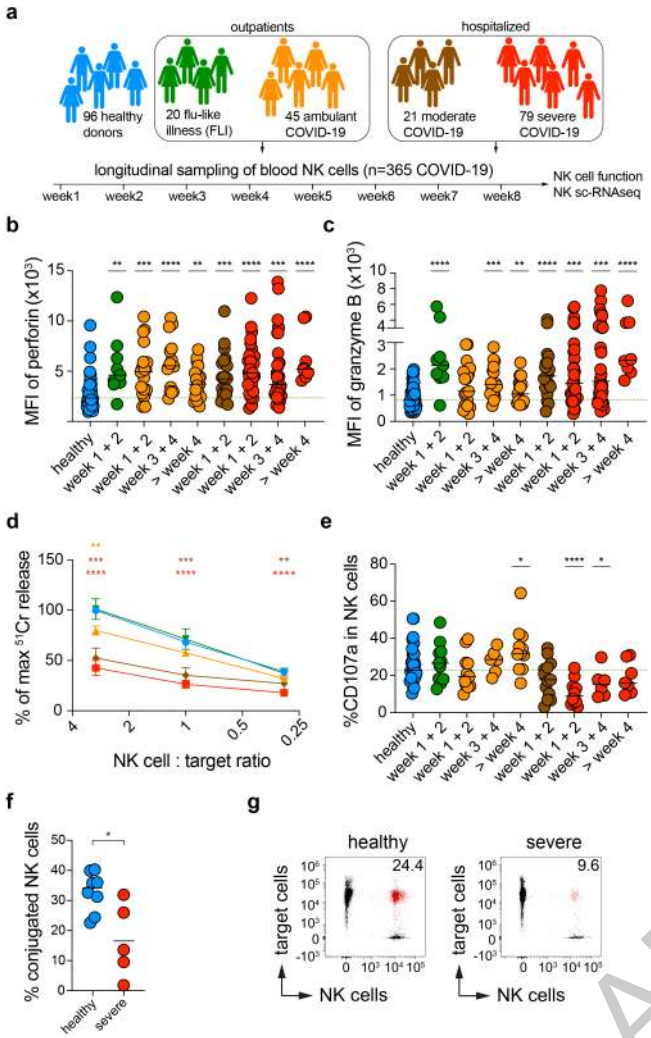

Fig. 2 | Impaired NK cell-mediated cytotoxicity during severe COVID-19. (**a**) Overview of study design. (**b,c**) Mean fluorescence intensity (MFI, median ± SEM) of perforin (**b**) and granzyme B (**c**) in CD56^{dim} NK cells. Independent measurements from 44 (**b**) or 50 healthy donors (**c**), 9 patients with flu-like illness (FLI), and from COVID-19 patients obtained 1 to 8 weeks after onset of symptoms (24 ambulant; n=56, 17 moderate; n=19, 30 severe; n=73). (**d**) Specific lysis (mean ± SEM) of K562 target cells by NK cells from the indicated donors obtained within the first 2 weeks after symptom onset was determined in a ^{51}Chromium release assay. Data represent pooled data of 12 independent experiments using 18 healthy donors (n=38 independent measurements), 8 patients with FLI (n=8) and 28 patients with COVID-19 (7 ambulant, n=7; 14 moderate, n=15; 10 severe, n=10). (**e**) Peripheral blood mononuclear cells of the indicated donor groups were co-cultured for 4h with K562 cells and the percentage (median ± SEM) of CD107a$^+$ NK cells was measured. Patients receiving corticosteroid treatment were excluded from the analysis. Data depict independent measurements across the disease course (29 healthy, n=29; 11 FLI, n=11; 21 ambulant COVID-19, n=28; 13 moderate COVID-19, n=13; 16 severe COVID-19, n=22). (**f,g**) quantification (**f**) and representative flow cytometry plots (**g**) of conjugation of NK cells from healthy donors (n=8) and from patients with severe COVID-19 (n=5) with target cells. Number indicates the frequency in percent of NK cells conjugated to target cells out of all NK cells (pooled data from two independent experiments). For **b,c,e** statistical analysis (indicated group *vs.* healthy) was performed using a One-way ANOVA followed by a two-sided Mann-Whitney U test. The dashed line indicates median frequency or MFI of NK cells from healthy donors. For (**d**) and (**f**) two-sided Mann-Whitney U test (**f**, p=0.03).

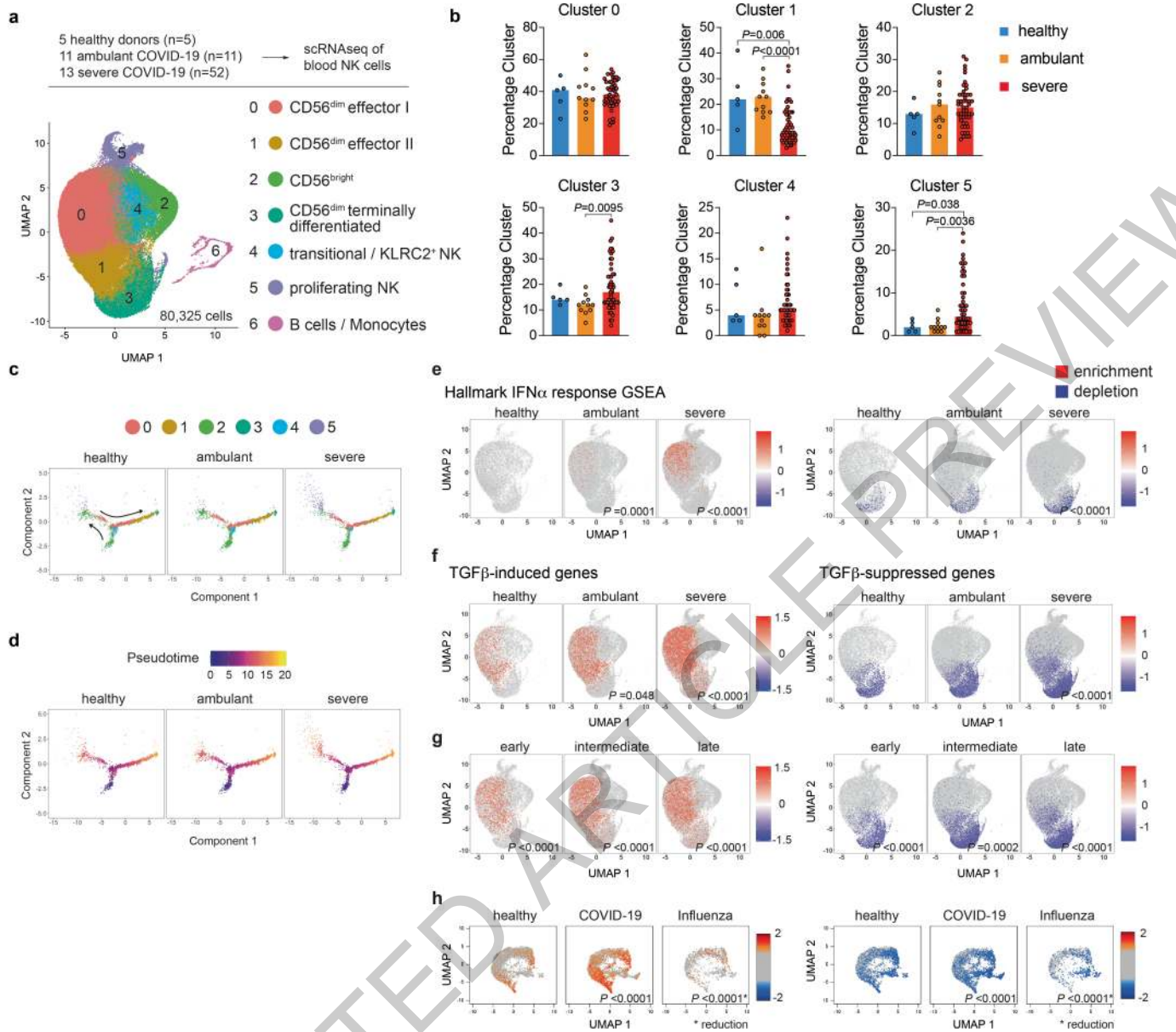

Fig. 3 | A TGFβ response signature is a hallmark of NK cells in severe COVID-19 but not in severe Influenza. (**a**-**g**) Single cell RNA-seq of highly purified peripheral blood NK cells of indicated donors and patients from d2 to d68 after symptom onset (Supplementary Table 1-3). Gating strategy depicted in Extended Data Fig. 8a. (**a**) UMAP representation of 80,325 sorted NK cells from all samples (n=68). Colors indicate unsupervised clustering. (**b**) Percentages (median) of cells allocated to each cluster in indicated groups. Each dot represents one sample subjected to scRNA-seq. P-values determined by One-way ANOVA followed by a two-sided Mann-Whitney U test. (**c**,**d**) Pseudotime trajectories (**c**) and representation of the individual NK cell clusters in trajectories (**d**) of 11,613 randomly selected NK cell transcriptomes from all groups. (**e**-**g**) Single cell gene set enrichment analysis (GSEA) of indicated gene sets was projected on the UMAP analysis (clusters 0, 1 and 3 only). Single cells with enriched gene expression displayed as red dots (left), cells with depletion of the genes displayed as blue dots (right). All sequenced NK cells per group are displayed as grey dots in the background. (**e**) IFNα response GSEA. (**f**,**g**) Enrichment of TGFβ-induced genes and depletion of TGFβ-suppressed genes in indicated groups (**f**) and across the course of severe COVID-19 (**g**; early: <day 14 after symptom onset, intermediate: day 15-28, late: > day 28). (**h**) NK cells were extracted from a publicly available single cell data set of PBMC from healthy donors, patients with COVID-19 or with severe influenza[30] and a single cell GSEA of the NK cell-specific TGFβ response gene set was performed as described in (**e**). GSEA p-values calculated by two-sided Fisher's exact test comparing the indicated groups with the left-sided (in **e** early was compared to healthy). P-value* describes a reduction in enrichment or depletion.

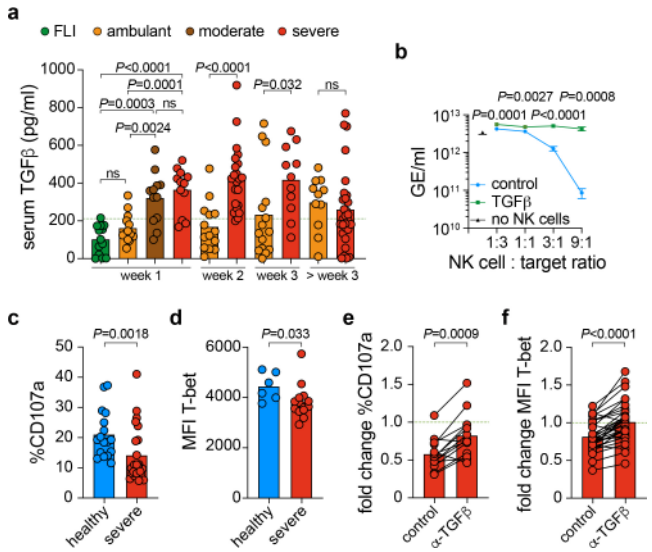

Fig. 4 | Serum of severe COVID-19 patients inhibits NK cell function in a TGFβ-dependent manner. (**a**) Serum levels of active TGFβ. Independent measurements from 13 patients with FLI (n=13) and 66 COVID-19 patients (30 severe ;n=74, 7 moderate; n=12, 39 ambulant; n=53) at indicated timepoints after symptom onset (group > 3 weeks contains samples from week 4 and 5). Dashed line indicates median TGFβ serum level of 34 healthy controls. Patients receiving corticosteroids were excluded. (**b**) NK cells from healthy donors cultured in medium containing IL-12/IL-15 with (green) or without TGFβ (blue) were co-cultured with SARS-CoV-2-infected Vero E6 cells. Viral load (mean ± SEM) was determined 12h later. Each data point represents NK cells from one individual donor (E:T 9:1 n=3, all others n=4, no NK cells n=11 samples). (**c,d**) Sorted NK cells from 3-9 healthy donors were cultured in medium containing either serum from a healthy donor or serum from a patient with severe COVID-19 (n=9 **c**; n=7 **d**) and the frequency of $CD107a^+$ NK cells after co-culture with K562 (**c**) or the MFI of T-bet (**d**) was determined. Each dot represents NK cells of one healthy donor cultured with serum of another healthy donor (blue, **c** n=17, **d** n=6) or of one patient with severe COVID-19 (red, **c** n=24, **d** n=14). (**e,f**) Sorted NK cells from 3-8 healthy donors were cultured in medium alone or with serum from patients with severe COVID-19. In a second condition, patient sera were pre-incubated with anti-TGFβ and then added as above. The frequency of $CD107a^+$ NK cells (**e**, n=14) and the MFI of T-bet (**f**, n=32) were determined. Fold change frequency or MFI between NK cells cultured in patients' sera (+/- prior anti-TGFβ treatment) and NK cells cultured in medium alone. (**e,f** two-sided Wilcoxon matched-pairs rank test, **a-d** two-sided Mann-Whitney U test).

Methods

Human donors

The recruitment of study subjects was approved by the Institutional Review Board of Charité (EA2/066/20, EA2/072/20, EAEA4/014/20 and EA2/092/20). Written informed consent was provided by all patients or legal representatives for participation in the study. Forty-five ambulant patients with COVID-19 (WHO 1 and 2 according to the WHO clinical ordinal scale), 21 hospitalized patients (WHO 3-4) with moderate COVID-19 and 79 patients with severe COVID-19 requiring ventilation (WHO 5-7, 52 of which fulfilling ARDS criteria according to the Berlin definition of ARDS[40]) were enrolled in this study. All COVID-19 patients were tested positive for SARS-CoV-2 RNA via nasopharyngeal swabs. Twenty patients that presented with flu-like symptoms but were tested negative for SARS-CoV-2 (FLI) and a total of 96 healthy donors who did not present any clinical sign of viral infection were enrolled as controls. Clinical characteristics of all subjects are summarized in Supplementary Table 1-3. For autopsy, informed consent was given by the next of kin, and autopsies were performed on the legal basis of §1 SRegG BE of the autopsy act of Berlin and §25(4) of the German Infection Protection Act. The sequencing of the post-mortem tissue was approved by the Ethics Committee of the Charité (EA2/066/20, EA1/144/13 and EA1/075/19 to Helena Radbruch) as well as by the Charité-BIH COVID-19 research board and complied with the Declaration of Helsinki. Additional use of anonymized clinical data is covered by section 25 of the Berlin Hospital Law and did not require further ethical or legal clearance.

Isolation of peripheral blood mononuclear cells and serum

Peripheral blood was drawn from each donor into EDTA Collection Tubes and for selected samples (CD107a assay) into heparin tubes (BD Biosciences, Plymouth, U.K.). Peripheral blood mononuclear cells (PBMC) were separated from peripheral blood by Pancoll human (PAN-Biotech) density gradient centrifugation at room temperature (RT). Cells were either used directly for analysis or stored in heat-inactivated fetal bovine serum (FCS, Pan-Biotech Cat# P30-3602) with 10% DMSO at -80 °C prior to analysis. Serum samples were drawn from each donor into Vacutainer® SSTTM tubes (BD Biosciences, Plymouth, U.K.), centrifuged for 10min at 2000 x g and stored at -20 °C prior to analysis.

Flow cytometry analysis

PBMCs were incubated with Fc Blocking Reagent (Miltenyi Biotec) according to manufacturer's instructions. To exclude dead cells, the cells were stained with a LIVE/DEAD (LD) Fixable Aqua Dead Cell staining Kit (ThermoFisher, Cat# L34965). For surface antigen staining the cells were incubated with monoclonal anti-human antibodies (Supplementary Table 4) for 20min at 4 °C. The Foxp3 Transcription Factor Staining Buffer Set (eBioscience, Cat# 00-5523-00) was applied prior to intracellular staining of transcription factors, cytotoxic molecules and cytokines. The samples were analyzed using FACS Fortessa X20 (BD Biosciences). Data was analyzed using FlowJo Software V10.3 (Treestar). Mean fluorescent intensity (MFI) values of NK cell populations were normalized to the MFI of lineage-negative marker-negative cells[41]. For intracellular cytokine staining of IFNγ (BioLegend, Cat# 502527) and TNF (BioLegend, Cat# 502908) NK cell were stimulated for 4h at 37 °C in the presence of brefeldin A (Sigma-Aldrich) with PMA (25ng/ml, Sigma-Aldrich) and ionomycin (500ng/ml, Sigma-Aldrich). Alternatively, NK cells were co-cultured with K562 target cells (ATCC CCL-243, verified by ATCC) for 4h at 37 °C in the presence of brefeldin A. In Supplementary Table 4, all antibodies are listed and assigned to staining panels A, B, C, D and E. Patient information and time-point after onset of symptoms when the peripheral blood was obtained for each flow cytometry analysis are listed Supplementary Tables 1-3.

In vitro culture of sorted NK cells

Frozen PBMCs were gradually thawed at 37 °C and resuspended in RPMI medium (GIBCO, Cat# 31870074), for all experiments supplemented with 20% heat-inactivated FCS (Fetal bovine serum, Pan-Biotech Cat# P30-3602), L-glutamine (200mM, GIBCO, Cat# 25030081), Penicillin/Streptomycin (10000U/ml, GIBCO, Cat# 15140122) and Gentamicin (Lonza BioWhittaker, Cat# BW17-519L). Live cells were discriminated using a LIVE/DEAD Fixable Aqua Dead Cell staining Kit (ThermoFisher, Cat# L34965) and incubated in human Fc Blocking reagent (Milteniy Biotec) according to manufacturer's instruction. The cells were stained with following anti-human antibodies for 20min at 4 °C: CD3 (eBioscience; Cat# 11-0039-42), CD4 (eBioscience; Cat# 11-0048-42), CD14 (BioLegend; Cat# 325604), CD19 BioLegend; Cat# 363008), CD45 (BioLegend; Cat# 393409), CD7 (BioLegend; Cat# 343119) and CD56 (BioLegend; Cat# 362511). NK cells were sorted as $LD^- Lin^-$ (CD3, CD4, CD14, CD19) $CD45^+ CD7^+ CD56^+$ using a FACS Aria II Cell Sorter (BD Biosciences).

Sorted NK cells were cultured in RPMI containing rh-IL12 (20ng/ml; PeproTech, Cat# 200-12H), rh-IL15 (20ng/ml; PerproTech, Cat# 200-15), rh-TGFβ (10ng/ml;PeproTech, Cat# 100-21), rh-IFNα (10,000 U/ml; RNDsystems, Cat# 11100-1) or rh-IFNβ (20ng/ml; RNDsystems, Cat# MAB1835-SP) and cultured for 2-4d at 37 °C with 5% CO_2 as indicated.

Chromium release assay

A chromium release assay was performed as previously described[42]. In brief, full PBMCs were cultured overnight in RPMI supplemented with rh-IL12 and rh-IL15. For selected analyses rh-TGFβ was added. NK cell frequencies in the PBMC fraction were determined using flow cytometry. K562 target cells were radioactively labeled by incubating 2 x 10^6 K562 cells in 450µl RPMI with 50µl of ^{51}Cr (CR-RA-8, Cr51, 185MBq, 5mCi/ml) for 2h at 37 °C on a rotator. After labeling, target cells were washed twice with RPMI before adding PBMC at indicated NK: target cell ratios (9:1, 3:1, 1:1 and 1:3). Following a co-culture of 4h (37 °C with 5% CO_2) the supernatant was collected and the ^{51}Cr released was quantified using a Wallac Wizard 1470 gamma counter. In order to quantify the maximal ^{51}Cr release for each experiment, the gamma count of the supernatant of target cells cultured without effector cells (spontaneous ^{51}Cr release) was subtracted from the gamma signal of labeled target cells only. The percentage of specific lysis (%lysis) or the percentage of ^{51}Cr release induced by healthy donors in a 3:1 NK cell : target ratio (% of max ^{51}Cr release) was calculated for each sample, respectively.

Degranulation assay of NK cells

CD107a expression on NK cells of the PBMC fraction was measured as described[43] (protocol 2 of the consensus protocol). Briefly, PBMCs were cultured at 2 x 10^6/ml in RPMI overnight. NK cells were subsequently co-cultured for 2h with K562 cells and stained for CD107a (eBioscience, Cat# 11-1079-42), CD56 (Beckman Coulter, Cat# A82943), CD8 (Beckman Coulter, Cat# IM2469), CD3 (Beckman Coulter, Cat# A94680) and CD45 (Beckman Coulter, Cat# B36294). The samples were analyzed on a Navios-EX FACS (Beckman Coulter). Data was analyzed using the Navios 2.0 software. CD107a mobilization of sorted NK cells (as described in section *In vitro culture of sorted NK c*ells) cultured in RPMI supplemented with rh-IL12/ rh-IL15 and rh-TGFβ as indicated, was analyzed after co-culture with K562 cells at a 2:1 NK: target cell ratio for 4h at 37 °C. Subsequently, cells were re-stained with a LIVE/DEAD Fixable Aqua Dead Cell staining Kit, human Fc Blocking reagent and the following antibodies: CD3 (eBioscience; Cat# 11-0039-42), CD4 (eBioscience; Cat# 11-0048-42), CD14 (BioLegend; Cat# 325604), CD19 (BioLegend; Cat# 363008), CD45 (BioLegend; Cat# 393409), CD7 (BioLegend; Cat# 343119), CD107a (BD Bioscience; Cat# 562622), CD56 (BioLegend; Cat# 362511), CD16 (BD Bioscience; Cat# 563785). The frequency of CD107a expression was determined in $LD^- Lin^-$ (CD3, CD4, CD14, CD19) $CD45^+ CD7^+ CD56^+$ NK cells using a FACS Fortessa X20 (BD Biosciences).

Conjugation assay

NK cell : target cell adhesion was assessed as previously described[44]. In brief, PBMCs were separated from peripheral blood by a density gradient as described above. Cells were enriched by negative selection, using the NK cell isolation kit (Miltenyi Biotec) according to manufacturer's instructions. After isolation, NK cells were labeled for 20min with Cell-trace Far Red Cell Proliferation Kit (Invitrogen, Cat# C34564) according to manufacturer's instructions. K562 target cells were labeled for 10min at 37 °C with Cell Proliferation Dye (Invitrogen, Cat# 65-0842-85). After labeling, cells were washed with RPMI, mixed in a 1:4 NK cell: target cell ratio and centrifuged at 300g for 1s. Cells were co-cultured for 1h at 37 °C before conjugates were quantified via flow cytometry.

Co-culture of NK Cells with SARS-CoV-2 infected cells

PBMCs were separated from freshly drawn peripheral blood by a density gradient as described above. Cells were enriched by negative selection using the NK cell isolation kit (Miltenyi Biotec) according to manufacturer's instructions. Enrichment was ensured by flow cytometry. After isolation, NK cells were stimulated 24-48h in RPMI 1640 supplemented with rh-IL12 (PeproTech, Cat# 200-12H), rh-IL15 (PerproTech, Cat# 200-15) and rh-TGFβ (PeproTech, Cat# 100-21) as indicated at 37 °C with 5% CO_2. NK cells were washed with DMEM and cocultured with SARS-CoV-2 infected Vero E6 (Cercopithecus aethiops; kidney epithelial cells; ATCC CRL-1586; verified by ATCC) or Calu-3 (human bronchial epithelial cells; ATCC HTB-55; verified by ATCC) as indicated. 175,000 VeroE6 and 300,000 Calu-3 cells per well were seeded in 24-well plates 24h prior to infection as indicated.

For masking experiments, NK cells were incubated with neutralizing antibodies anti-NKp30 (clone F252), anti-NKp44 (clone KS38), anti-NKp46 (clone KL247), anti-NKG2D (clone BAT221 and clone ON72), anti-DNAM-1 (clone F5), anti-2B4 (clone CO54) at RT 45min prior to co-culture as indicated. For all blocking experiments, target cells were incubated with anti-HLA-I (clone A6/136). mAbs were kindly provided by E. Marcenaro (University of Genova, Italy).

Cells were infected with the SARS-CoV-2/München 984 virus isolate (B.1 lineage, hCoV-19/Germany/BY-ChVir-984/2020, accession ID: EPI_ISL_406862; Pango lineage version 3.1.1, lineages version 2021-06-15) or the variant B.1.351 (hCoV-19/Germany/BW-ChVir22131/2021, accession ID: EPI_ISL_862149), cell culture passage 2 (ref. [45]) with an MOI of 0.001 (Vero E6) and an MOI of 0.1 (Calu-3). Virus was diluted in Opti-Pro serum-free medium (Thermo Fisher). For infection, supernatant was removed, cells were rinsed once with 0.5 ml PBS (Thermo Fisher) and 200µl of virus-containing dilution was inoculated on the cells for 1h at 37 °C. Next, 500µl of NK cell suspension was added either 12h post infection (hpi) as indicated. Adherent cells were harvested 12h (Vero E6) or 24h (Calu-3) after NK cell addition for isolation of viral RNA. For isolation of viral RNA, 35µl of MagNA Pure 96 external lysis buffer (Roche, Penzberg, Germany) was added to the adherent cells. All samples were heat-inactivated for 10min (minutes) at 70 °C. Isolation and purification of viral RNA was performed using the MagNA Pure 96 System (Roche, Penzberg, Germany) according to the manufacturers' recommendations. Viral RNA was quantified using real-time RT-PCR (E gene assay) as previously described[46]. All infection experiments were done under biosafety level 3 conditions with enhanced respiratory personal protection equipment.

Viral load data analyses

Viral load (RNA copies per swab) measurements were obtained based on a calibrated curve of viral RNA copies and RT-PCR cycle threshold values, as described in Jones *et al.*[47] For the examination of temporal viral load dynamics, patients with at least two viral load measurements and two immune cell count measurements were included, and a linear regression was calculated. A maximum offset for both parameters was set to 7 days and only infections with a duration of less than 40 days were considered. Regression analysis was performed using the seaborn (regplot) package version 0.11.1 and the scipy (stats.linregress) package (version 1.6.0) running under Python 3.9.1. For indicated analyses, patients were categorized as having either low or normal absolute immune cell counts, according to whether their first immune cell count had a value below or above a threshold value. Thresholds: NK cells 40/µl; B cells 40/µl; T cells 360/µl; $CD4^+$ T cells 200/µl; $CD8^+$ T cells 300/µl; lymphocytes ($CD45^+$, $CD14^-$) 600/µl. Analysis was performed on hospitalized patients who tested positive (via SARS-CoV-2 RT-PCR), including patients who tested positive in an ICU ward at any point during their infection and including severe COVID-19 patients of the study cohort (Extended Data Fig. 1, Supplementary Table 3).

NK cell isolation from peripheral blood for single cell sequencing

Frozen PBMCs from 13 patients with severe COVID-19 (52 samples), 11 ambulant COVID-19 patients (11 samples) from day 2 to day 68 after onset of symptoms (Supplementary Tables 1-3) and from 5 healthy donors (5 samples) were thawed in RPMI (GIBCO, Cat# 31870074) supplemented with 20% heat-inactivated FCS and incubated with Fc Blocking Reagent (Miltenyi Biotec) following manufacturer's instructions. Up to 1×10^7 cells per 100µl were stained with the following anti-human antibodies: CD3 (Miltenyi Biotec, Cat# 130-113-133), CD14 (Miltenyi Biotec, Cat# 130-113-152), CD19 (Miltenyi Biotec, Cat# 130-113-172), CD45 (BioLegend, Cat# 304008) and CD56 (Miltenyi Biotec, Cat# 130-113-305). To allow cell pooling, each sample was also incubated with one of eight different TotalSeq-C anti-human Hashtags (LNH-94;2M2, Barcoded, BioLegend, Cat# 394661, 394663, 394665, 394667, 394669, 394671, 394673 and 394675). DAPI was added before sorting to allow for dead cell exclusion. NK cells were identified and sorted as $DAPI^-$ $CD3^-$ $CD14^-$ $CD19^-$ $CD45^+$ $CD56^+$. All sortings were performed using a MA900 Multi-Application Cell Sorter (Sony Biotechnology). Cell counting was performed using a MACSQuant flow cytometer (Miltenyi Biotec). Sorted NK cells were further processed for single cell RNA sequencing.

For the generation of an NK cell-specific TGFβ-response data set live cells in thawed PBMCs were discriminated using a LIVE/DEAD Fixable Aqua Dead Cell staining Kit (ThermoFisher, Cat# L34965) and incubated in human Fc Blocking reagent (Miltenyi Biotec) according to manufacturer's instruction. The cells were stained with following anti-human antibodies for 20min at 4 °C: CD3 (eBioscience; Cat# 11-0039-42), CD4 (eBioscience; Cat# 11-0048-42), CD14 (BioLegend; Cat# 325604), CD19 BioLegend; Cat# 363008), CD45 (BioLegend; Cat# 393409), CD7 (BioLegend; Cat# 343119) and CD56 (BioLegend; Cat# 362511). NK cells were sorted as LD^- Lin^- (CD3, CD4, CD14, CD19) $CD45^+$ $CD7^+$ $CD56^+$ using a FACS Aria II Cell Sorter (BD Biosciences). Sorted NK cells were cultured in RPMI containing rh-IL12 and rh-IL15 with or without additional rh-TGFβ for 4d at 37 °C with 5% CO_2 prior to single cell RNA sequencing.

Single cell RNA-library preparation and sequencing

The 10X Genomics workflow for cell capturing and scRNA gene expression (GEX) was applied to sorted NK cells using the Chromium Single Cell 5' Library & Gel Bead Kit as well as the Single Cell 5' Feature Barcode Library Kit (10X Genomics). Final GEX was obtained after fragmentation, adapter ligation and final Index PCR using the Single Index Kit T Set A. Qubit HS DNA assay kit (life technologies) was used for library quantification and fragment sizes were determined using the Fragment Analyzer with the HS NGS Fragment Kit (1-6000bp) (Agilent). Sequencing was performed on a NextSeq500 device (Illumina) using High Output v2 Kits (150 cycles) with the recommended sequencing conditions for 5' GEX libraries (read1: 26nt, read2: 98nt, index1: 8nt).

Single-cell transcriptome analysis

Chromium single cell data were processed using cellranger-3.1.0. The mkfastq and the count pipeline were used in default

parameter settings for demultiplexing, alignment of reads to the Refdata-cellranger-hg19-1.2.0 genome, barcode and UMI counting and calling of intact cells. The number of expected cells was set to 3000. Further analysis was performed using the Seurat R-package (version 3.1.1)[48]. The pooled samples were separated using 8 cite-seq hashtags (TotalSeq-C, Biolegend). Cells with more than 30% cite-seq reads for a particular hashtag were assumed as positively stained. Cells with no (undefined origin) or ambivalent assignments (doublets) were removed from further analysis. The resulting transcriptome profiles of NK cells from healthy donors, ambulant and severe COVID-19 patients were normalized and integrated as described[49]. Variable genes were detected and scaled. Data was scaled and an *Uniform Manifold Approximation and Projection* (UMAP) was performed in default parameter settings using Scale Data, RunPCA and RunUMAP with 30 principal components. Quality control was performed by visual inspection of the fraction of mitochondrial genes, number of detected genes and UMI counts per cell. No noticeable abnormalities were observed. Transcriptionally similar cells were clustered using shared nearest neighbor (SNN) modularity optimization with a SNN resolutions of 0.2. Marker genes for clusters were identified using FindAllGenes with a log fold change > 2.5 and a minimum of 0.1 expressing cells. The genes were used for manual annotation of clusters' function informed by previous publications[16,20,48,50]. One out of 6 clusters revealed B cell and monocyte-specific genes (CD19, CD14) and was excluded from further analysis.

Pseudotime trajectory analysis was performed using Monocle2 R Package. Cells from each group (healthy, ambulant and severe COVID-19) were randomly down sampled to an equal depth of 3871 cells. The overall 11613 cells were used for the calculation in monocle2. The top 1000 DEGs across the five clusters (ranked by lowest q-value) were used to order the cells. The BEAM method was used to identify genes that significantly differ in expression level across a branch point[22].

Single cell data derived from NK cells cultured in presence and absence of TGFβ were analyzed using the analog workflow except for clustering and trajectory analysis steps. The TGFβ response signature was defined based on differentially expressed genes between samples with and without TGFβ treatment. For comparison of samples, the two-sided Mann-Whitney U Test was used on log-normalized counts. Differentially expressed genes were identified (adj. $p \leq 0.05$ and a log fold change > 2.2 for enrichment and < 2.2 for depletion). The heatmap of DEG is based on z-transformed means of log-normalized counts. The hierarchical clustering was performed using Euclidian distances and WARD linkage criterium. All generated sequencing data was deposited at NCBI Gene Expression Omnibus (Accession No.: GSE184329).

Analysis of peripheral blood NK cells from COVID-19 and influenza patients in a publicly available data set

NK cells were extracted from a publicly available PBMC single-cell sequencing dataset (GSE149689) consisting of 4 healthy, 11 COVID-19 and 5 severe influenza samples[30]. In the first step the individual samples and 59,572 cells were integrated and subdivided into 10 clusters in a UMAP representation with a SNN resolution of 0.1. A heat map of cell type defining genes was used to identify 10,604 NK cells from the PBMC. GSEA analysis for TGFβ-induced and TGFβ-suppressed NK cell genes was performed as described below.

Analysis of non-hematopoietic and hematopoietic cell populations from lung tissue of COVID-19 and non-SARS-CoV-2 pneumonia patients in a publicly available data set

The lung single nuclei dataset (EGA Ref ID: EGAS00001004689) consisting of 3 control subjects deceased from pneumonia unrelated to COVID-19 and 7 patients deceased from COVID-19 associated pneumonia[31] was aligned to an hg19 reference transcriptome that included the SARS-CoV-2 genome (Refseq-ID: NC_045512) using cellranger v3.0.1 (10X Genomics). Ambient RNA removal was performed with SoupX v1.4.5[51]. First, the 10 samples and 53,709 cells were integrated as previously described for the NK cell single-cell sequencing data set and subdivided into 33 clusters in a UMAP representation with a SNN resolution of 1. A heat map of 13 genes was used to identify the NK cells from the lung, and cluster 25 was defined as the NK cell-specific cluster of 845 cells. Remaining cell populations were identified according to Gassen *et al.*[31]

Gene set enrichment analysis (GSEA)

GSEA was performed for each cell based on differences in log-normalized counts to the mean of all cells analyzed using 1000 randomizations (FDR < 0.5 and normalized p-value < 0.2)[52]. For visualization, the normalized enrichment score per cell within the indicated gene set (up or downregulation) was plotted. Gene sets (Hallmark, REACTOME and KEGG) were obtained from Molecular Signatures Database (MSigDB, version 6.2)[53,54]. The NK cell-specific TGFβ response gene set was newly generated in this study. The GSEA-enrichment plot (score curve) of TGFβ-suppressed genes in lung tissue-resident NK cells was performed on pre-ranked differences between medians of expressing cells in otherwise default parameter settings. Solely genes expressed in at least one group were considered. The median was set to 0 if no expressing cells were found.

In vitro NK cell exposure to patient serum

Sorted NK cells from healthy control patients were cultured for 48h in RPMI containing IL-12, IL-15 and IL-2 (25ng/ml, PeproTech; Cat# 212-12) as indicated and 20% of either serum from another healthy control patient (Supplementary Table 1) or from a patient with severe COVID-19 (Supplementary Table 3). If not stated otherwise, IL-12, IL-15 and serum were used. For indicated experiments the patient sera were pre-incubated with anti-TGFβ1, 2, 3 antibody (RND systems; Cat# MAB1835-SP), anti-IL6 (5µg/ml; RNDsystems; Cat# MAB206), anti-IL10 (30µg/ml; RNDsystems; Cat# MAB217), anti-IL15 (5µg/ml; eBioscience; Cat# 16-0157-82) as indicated for 10min before being added to the culture otherwise using identical culture conditions. After 48h, protein expression levels of T-bet were measured, the frequency of CD107a expression in NK cells was analyzed after 4h co-culture with K562 cells using flow cytometry or viral replication was determined, as described above.

Cytokine measurements

Cytokine levels were measured using a bead-based multiplex cytokine array (Human Cytokine 25-Plex ProcartaPlex Panel 1B, Thermo Fisher Scientific). Prior to the assay, serum samples were diluted 1:3 in dilution buffer provided with the kit. TGF-β was detected using the Human TGFβ1 Simplex ProcartaPlex Kit (Thermo Fisher Scientific). Prior to measuring serum-TGFβ1, the bioactive form of TGFβ1 was generated by incubating the serum with 1N HCl followed by neutralization with 1.2N NaOH according to the manufacturer's instructions. The samples were incubated with antibody coated magnetic beads for 30min at RT with shaking, then incubated overnight at 4 °C followed by a 1h incubation period at RT. All following incubation steps were performed according to the manufacturer's instructions. The assay plates were read using the Luminex MAGPIX system and quantified using the xPONENT analysis software (Luminex Corporation). IFNα serum concentration was analyzed using Simoa® IFNα Advantage Kit (Quanterix) according to the manufacturer's instructions.

Statistical analysis and reproducibility

All statistical tests were performed with Graph Pad Prism V7 software as indicated for each analysis (*$p \leq 0.05$, **$p \leq 0.01$, ***$p \leq 0.001$, and ****$p \leq 0.0001$; ns, not significant). Representative data of at least 3 independent experiments shown in Figure 1d,e,g; Figure 2f; Figure 4c,f; Extended Data Fig. 15a,b,c,d. Representative data of 2 independent experiments shown in Extended Data Fig. 15j,k,n,o.

Reporting summary

Further information on research design is available in the Nature Research Reporting Summary linked to this paper.

Data availability

All generated sequencing data was deposited at NCBI Gene Expression Omnibus (Accession No. GSE184329).

40. Force, A. D. T. et al. Acute respiratory distress syndrome: the Berlin Definition. *JAMA* **307**, 2526-2533, https://doi.org/10.1001/jama.2012.5669 (2012).
41. Cossarizza, A. et al. Guidelines for the use of flow cytometry and cell sorting in immunological studies (second edition). *Eur J Immunol* **49**, 1457-1973, https://doi.org/10.1002/eji.201970107 (2019).
42. Verneris, M. R., Karimi, M., Baker, J., Jayaswal, A. & Negrin, R. S. Role of NKG2D signaling in the cytotoxicity of activated and expanded CD8+ T cells. *Blood* **103**, 3065-3072, https://doi.org/10.1182/blood-2003-06-2125 (2004).
43. Bryceson, Y. T. et al. A prospective evaluation of degranulation assays in the rapid diagnosis of familial hemophagocytic syndromes. *Blood* **119**, 2754-2763, https://doi.org/10.1182/blood-2011-08-374199 (2012).
44. Deguine, J., Breart, B., Lemaitre, F., Di Santo, J. P. & Bousso, P. Intravital imaging reveals distinct dynamics for natural killer and CD8(+) T cells during tumor regression. *Immunity* **33**, 632-644 (2010).
45. Wolfel, R. et al. Virological assessment of hospitalized patients with COVID-2019. *Nature* **581**, 465-469, https://doi.org/10.1038/s41586-020-2196-x (2020).
46. Corman, V. M. et al. Detection of 2019 novel coronavirus (2019-nCoV) by real-time RT-PCR. *Euro Surveill* **25**, https://doi.org/10.2807/1560-7917.ES.2020.25.3.2000045 (2020).
47. Jones, T. C. et al. Estimating infectiousness throughout SARS-CoV-2 infection c ourse. *Science* **373**, https://doi.org/10.1126/science.abi5273 (2021).
48. Butler, A., Hoffman, P., Smibert, P., Papalexi, E. & Satija, R. Integrating single-cell transcriptomic data across different conditions, technologies, and species. *Nat Biotechnol* **36**, 411-420, https://doi.org/10.1038/nbt.4096 (2018).
49. Stuart, T. et al. Comprehensive Integration of Single-Cell Data. *Cell* **177**, 1888-1902 e1821, https://doi.org/10.1016/j.cell.2019.05.031 (2019).
50. Smith, S. L. et al. Diversity of peripheral blood human NK cells identified by single-cell RNA sequencing. *Blood Adv* **4**, 1388-1406, https://doi.org/10.1182/bloodadvances.2019000699 (2020).
51. Young, M. D. & Behjati, S. SoupX removes ambient RNA contamination from droplet-based single-cell RNA sequencing data. *Gigascience* **9**, https://doi.org/10.1093/gigascience/giaa151 (2020).
52. Subramanian, A. et al. Gene set enrichment analysis: a knowledge-based approach for interpreting genome-wide expression profiles. *Proc Natl Acad Sci U S A* **102**, 15545-15550, https://doi.org/10.1073/pnas.0506580102 (2005).
53. Li, S. et al. Molecular signatures of antibody responses derived from a systems biology study of five human vaccines. *Nat Immunol* **15**, 195-204, https://doi.org/10.1038/ni.2789 (2014).
54. Liberzon, A. et al. Molecular signatures database (MSigDB) 3.0. *Bioinformatics* **27**, 1739-1740, https://doi.org/10.1093/bioinformatics/btr260 (2011).
55. Sivori, S. et al. Human NK cells: surface receptors, inhibitory checkpoints, and translational applications. *Cell Mol Immunol* **16**, 430-441, https://doi.org/10.1038/s41423-019-0206-4 (2014) (2019).

Acknowledgements The authors are most grateful to the patients for their consent in participating in this study. We thank members of the Diefenbach laboratory, the Mashreghi laboratory, the Kruglov laboratory, the Klose laboratory and the Romagnani laboratory for valuable discussions on the manuscript. Masking antibodies against NKp30 (clone F252) and DNAM-1 (clone F5) were kindly provided by D. Pende (IRCCS Ospedale Policlinico San Martino, 16132 Genoa, Italy) and NKp46 (clone KL247) and NKp44 (KS38) by S. Parolini (Sezione di Oncologia e Immunologia Sperimentale, Dipartimento di Medicina Molecolare e Traslazionale, Università di Brescia). We are grateful to the Benjamin Franklin Flow Cytometry Facility (M. Fernandes and A. Branco) and the DRFZ flow cytometry facility (J. Kirsch, A.C. Teichmuller and T. Kaiser) for support in cell sorting. BFFC is supported by DFG Instrument Grants INST 335/597-1 FUGG und INST 335/777-1 FUGG. We are indebted to K. Oberle, F. Egelhofer, J. Heinze and A. Sebastiampillai for technical assistance and advice. We thank A. Bayindir, F. Cicek and E. Daka for support in the management of patient material. The work was supported by Deutsche Forschungsgemeinschaft (TR-SFB 84/A02 and A06, TR-SFB241/A01, SPP1937-DI764/7 to A.D.; TRR130/P16 and P17 to A.R. and H.R.; TR-SFB 84/A07 to C.D.; TRR241/A04 to A.K.; RA 2491/1-1 to H.R.; SFB-TR 84/B08, SFB 1449/Z02 to M.A.M), the European Research Council (ERC-2010-AdG 268978 to A.R.), Einstein Foundation Berlin (Einstein Professorship to A.D.), by the state of Berlin and the "European Regional Development Fund" to M.F.M. (ERDF 2014-2020, EFRE 1.8/11, Deutsches Rheuma-Forschungszentrum), the Berlin Institute of Health with the Starting Grant - Multi-Omics Characterization of SARS-CoV-2 infection, Project 6 "Identifying immunological targets in COVID-19" to A.D. and M.F.M., Russian Ministry of Science and Higher Education of the Russian Federation (grant 075-15-2019-1660) and Russian Foundation for Basic Research (#17-00-00435) to A.K., Leibniz Association (Leibniz Collaborative Excellence, TargArt) to T.K. and M.F.M., German Federal Ministry of Education and Research (BMBF) projects "NaFoUniMedCovid19" (FKZ: 01KX2021) – COVIM (AP-4) V.M.C., L.E.S. and A.D. RECAST (01KI20337) to B.S., V.M.C., L.E.S, J.R. and M.M.; 82DZL009B1 and 01IK20337 to M.A.M., and AIRC Foundation to E.M. T.C.J. is in part funded through NIAID-NIH CEIRS contract HHSN272201400008C. C.U.D. acknowledges support by a Rahel Hirsch Habilitationsstipendium. The autopsies were facilitated by the Biobank of the Department of Neuropathology, Charité-Universitätsmedizin Berlin and supported by the BMBF (Organostrat, Defeat Pandemics).

Author contributions M.W., C.T. and M.F.G. performed most experiments and analyzed the data. D.N. contributed to the experiments with SARS-CoV-2 infected cells. T.C.J performed viral load data analyses. T.H., P.N., S.M.E., I.M., U.K., C.M., C.D., A.K. and G.A.H., helped with experiments. F.H. and P.D. analyzed RNA sequencing data. S.F. and M.M. performed serum cytokine measurements. S.A., S.T., S.Z., E.V., F.K., L.E.S., L.H., M.A.M., V.M.C., R.L.C., T.A., B.S., J.R., T.S., C.C., H.R., T.K., V.M., K.A., T.S. supported the management of patient samples and clinical data. J.A.T., E.M., I.M. and C.D. helped with the design of *in vitro* experiments. M.W., C.T., M.F.M., and A.R. contributed to the development of the study concept. A.D. and M.F.M. designed, directed and supervised the study. A.D. wrote the manuscript with input from co-authors.

Competing interests The authors declare no competing interests.

Additional information

Supplementary information The online version contains supplementary material available at https://doi.org/10.1038/s41586-021-04142-6.

Correspondence and requests for materials should be addressed to Mario Witkowski or Andreas Diefenbach.

Peer review information *Nature* thanks the anonymous reviewers for their contribution to the peer review of this work. Peer review reports are available.

a

	COVID-19 Hospitalized				COVID-19 Intensive Care Unit				Severe COVID-19 study cohort			
	mean	median	SD	n	mean	median	SD	n	mean	median	SD	n
NK cells > 40/µl	-0.14	-0.12	0.32	250	-0.13	-0.12	0.31	183	-0.24	-0.16	0.51	42
NK cells ≦ 40/µl	-0.08	-0.09	0.19	29	-0.07	-0.07	0.18	23	-0.05	-0.09	0.12	5
T cells > 360/µl	-0.10	-0.12	0.27	222	-0.09	-0.11	0.22	160	-0.12	-0.14	0.22	32
T cells ≦ 360/µl	-0.24	-0.16	0.43	57	-0.24	-0.16	0.47	46	-0.42	-0.19	0.76	15
$CD4^+$ T cells > 200/µl	-0.11	-0.12	0.26	232	-0.10	-0.12	0.22	169	-0.13	-0.14	0.22	36
$CD4^+$ T cells ≦ 200/µl	-0.23	-0.16	0.47	47	-0.24	-0.15	0.52	37	-0.5	-0.20	0.86	11
$CD8^+$ T cells > 300/µl	-0.10	-0.12	0.27	195	-0.10	-0.12	0.21	140	-0.11	-0.14	0.23	27
$CD8^+$ T cells ≦ 300/µl	-0.20	-0.16	0.38	84	-0.19	-0.14	0.42	66	-0.36	-0.17	0.66	20
B cells > 40/µl	-0.12	-0.12	0.27	268	-0.12	-0.12	0.24	197	-0.17	-0.15	0.34	44
B cells ≦ 40/µl	-0.31	-0.14	0.67	15	-0.31	-0.10	0.80	10	-0.86	-0.14	1.25	3
lymphocytes > 600/µl	-0.11	-0.12	0.27	215	-0.1	-0.12	0.22	153	-0.13	-0.14	0.24	30
lymphocytes ≦ 600/µl	-0.22	-0.15	0.41	64	-0.22	-0.15	0.44	53	-0.37	-0.15	0.72	17

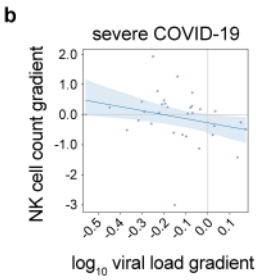

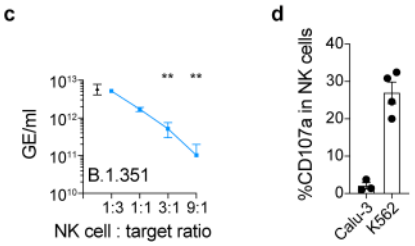

Extended Data Fig. 1 | The temporal viral load decline is related to the NK cell status. (**a**) Regressions for temporal viral load according to absolute peripheral blood immune cell count. The viral load trajectory was estimated by linear regression for COVID-19 patients with at least two viral load measurements each, and whose first absolute immune cell count was below or above the indicated threshold (see also methods). Analysis was performed on SARS-CoV-2 RNA-positive patients who were hospitalized, hospitalized and who tested positive on an ICU ward at any point during their infection (Intensive Care Unit group), and severe COVID-19 patients of the study cohort (Supplementary Table 3). The table lists the mean and median temporal viral load regression gradient, standard deviation (SD) and number of patients (n) per group. (**b**) The relationship between temporal gradient of $\log_{10}$ viral load and NK cell count change. For each of 32 severe COVID-19 patients with at least two viral load measurements and at least two NK cell count measurements, a linear regression was calculated for each series and a dot corresponding to the two gradients was plotted (n=32). The blue regression line in the center of the error band shows the correlation between temporal $\log_{10}$ viral load gradient and NK cell count gradient, with the shaded region indicating the 95% confidence region. The overall regression slope has -1.33 (standard error 0.9) and the correlation coefficient of the dots is -0.26. Two-sided Fisher's exact test p=0.029; Two-sided Chi-square p=0.018. (**c**) Vero E6 cells were infected with the B.1.351 variant of SARS-CoV-2. At 1h post infection, NK cells from healthy donors activated for 24h *in vitro* with IL-12/15 were added. Viral replication was measured 12h later as genome equivalents (GE)/ml (E:T 1:3 n=3 donors, all other E:T ratios n=4 donors, no NK cells n=8 samples, two-sided Mann-Whitney U test comparing E:T ratios *vs*. no NK cells, E:T 3:1; p=0.004, E:T 9:1; p=0.004). (**d**) Quantification of CD107a expression (mean ± SEM) in NK cells from healthy donors co-cultured 4h with Calu-3 or K562 cells (n=3 donors for Calu-3 cells and n=4 donors for K562).

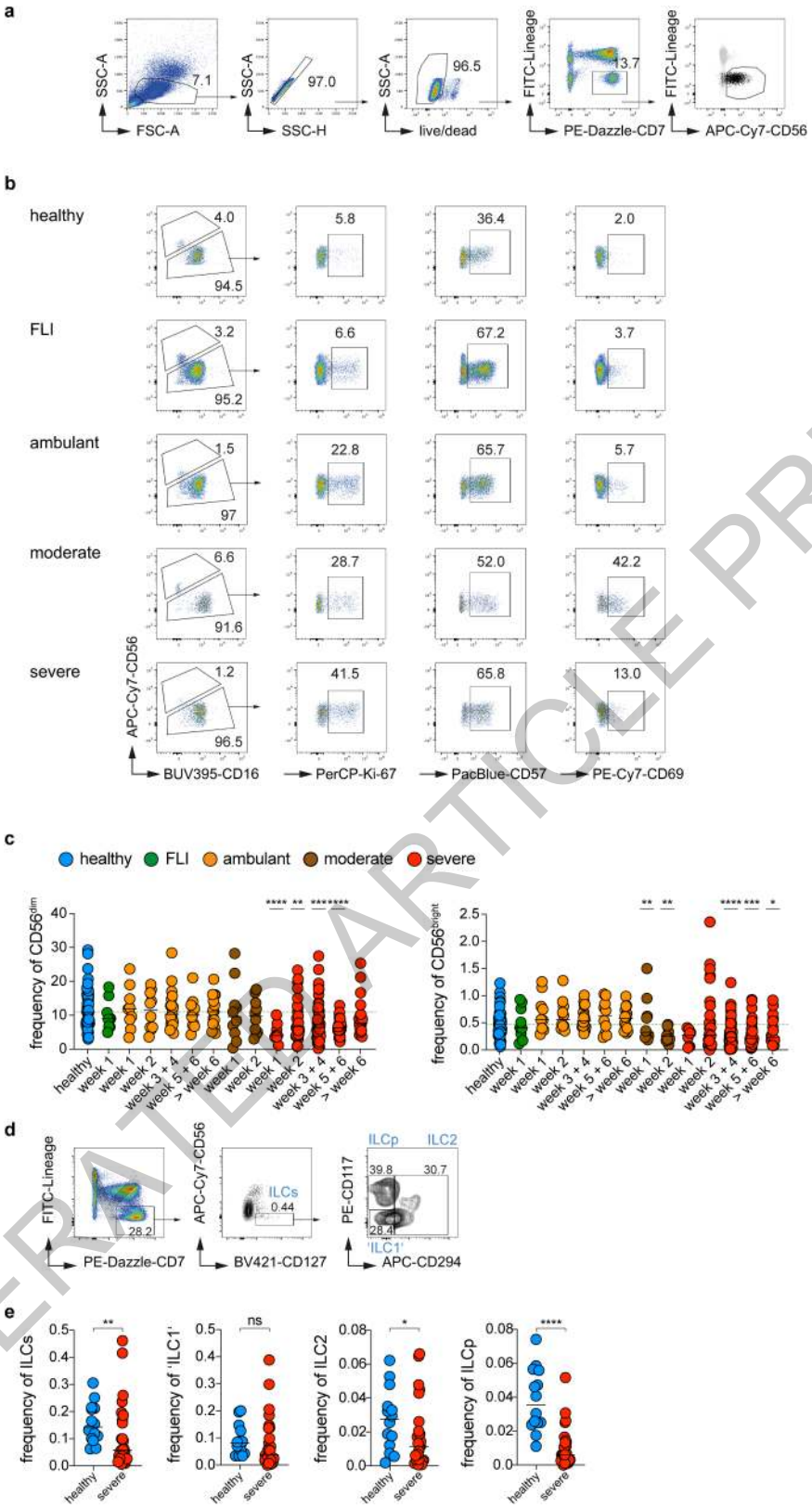

Extended Data Fig. 2 | See next page for caption.

Extended Data Fig. 2 | Reduction of peripheral blood NK cells and ILC1-like cells during COVID-19. (**a**) Gating strategy for the identification of $CD56^{bright}$ and $CD56^{dim}$ peripheral blood NK cells. (**b**) Continuation of the gating depicted in (**a**) and representative flow cytometry plots for the indicated markers in $CD56^{dim}$ NK cells of a healthy donor, patient with flu-like illness (FLI), ambulant patient with COVID-19, patient with moderate COVID-19 and a patient with severe COVID-19 (**b**). (**c**) Frequency of $CD56^{dim}$ and $CD56^{bright}$ NK cells (median ± SEM) in the peripheral blood of healthy donors and patients. Independent measurements of 53 healthy donors (n=53), 9 flu-like illness (FLI, n=9), 29 ambulant COVID-19 (n=62), 17 moderate (n=19) and 45 severe COVID-19 patients (n=133) between week 1 and week 11 after onset of symptoms. Statistical analysis was performed using a One-way ANOVA followed by a two-sided Mann-Whitney U test comparing healthy *vs*. FLI or COVID-19 groups. The dashed line indicates the median frequency in healthy donors. (**d,e**) Identification of ILC subsets in 14 healthy donors (n=14) and 8 patients with severe COVID-19 (n=28 independent measurements). (**d**) Gating strategy for ILC with pre-gate set on live, $CD45^{+}$ single lymphocytes. (**e**) Frequencies of indicated ILC subsets in both groups (independent measurements of two-sided Mann-Whitney U test, ILCs; p=0.007, 'ILC1'; p=0.09, ILC2; p=0.04, ILCp; p<0.0001) (*; $p \leq 0.05$, **; $p \leq 0.01$, ***; $p \leq 0.001$, ****; $p \leq 0.0001$).

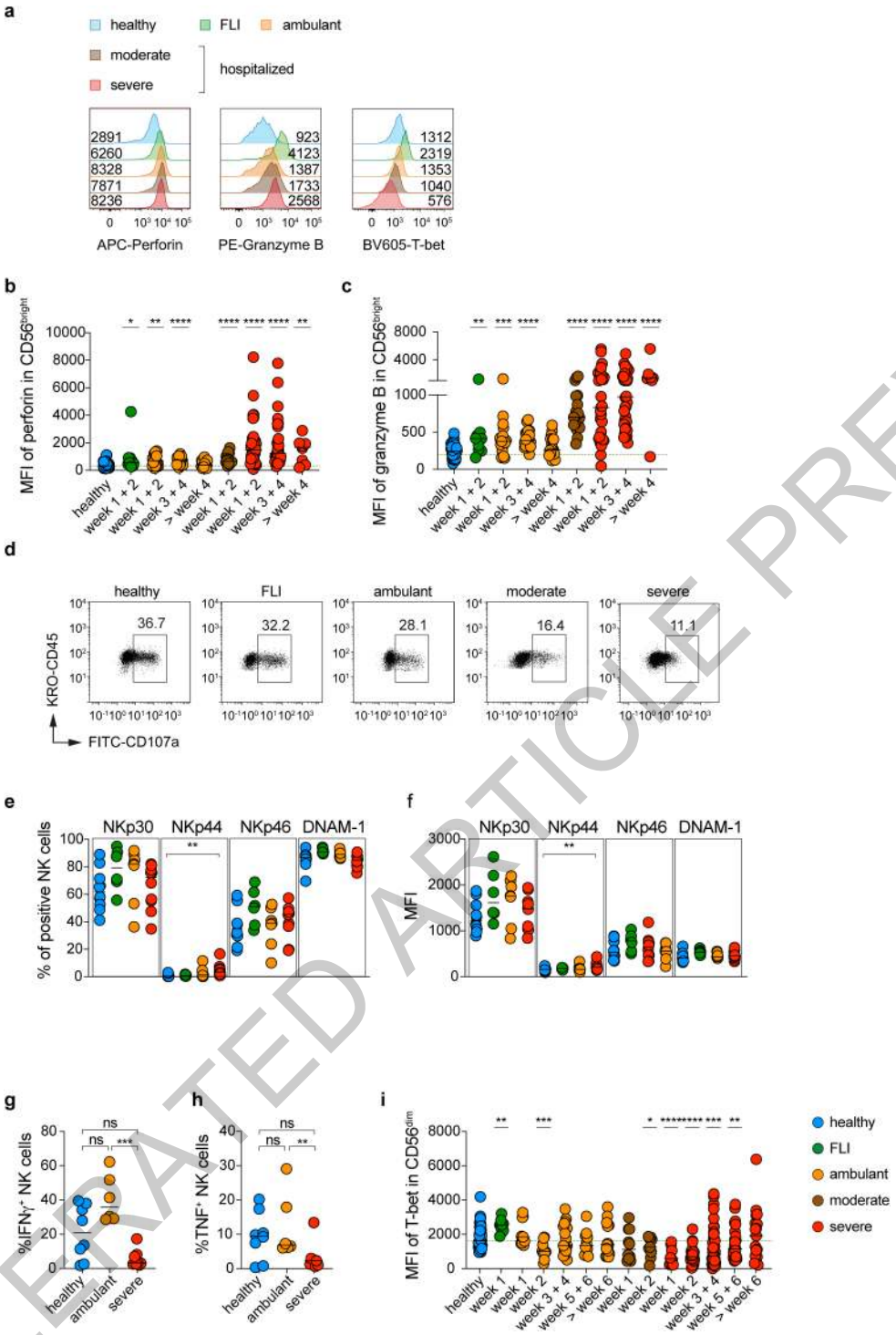

Extended Data Fig. 3 | See next page for caption.

Extended Data Fig. 3 | NK cells upregulate the expression of cytotoxic molecules but fail to express IFNγ and TNF during severe COVID-19. **(a)** Representative flow cytometry analysis showing the mean fluorescence intensity (MFI) of the indicated proteins in $CD56^{dim}$ NK cells from the indicated patient groups. (**b,c**) MFI of perforin (**b**) and granzyme B (**c**) in $CD56^{bright}$ peripheral blood NK cells. Independent measurements from 44 (n=44 for perforin) or 50 healthy donors (n=50 for granzyme B), 9 patients with FLI (n=9), 24 ambulant COVID-19 (n=56), 17 moderate COVID-19 (n=19) and 30 severe COVID-19 patients (n=73) from week 1 to 6 after onset of symptoms. **(d)** Representative flow cytometry plots of cell surface CD107a expression by NK cells from indicated groups after 4h co-culture with K562 cells. Pre-gate was set on $CD3^-$ $CD56^+$ lymphocytes. (**e,f**) Frequency of expressing NK cells (**e**) and MFI (**f**) of indicated immunoreceptors on NK cells of 9 healthy donors (n=9 independent measurements), 6 patients with FLI (n=6), 7 ambulant (n=7) and severe 9 COVID-19 (n=10) (Frequency of $NKp44^+$ NK cells healthy *vs*. severe p=0.004, MFI of $NKp44^+$ NK cells healthy *vs*. severe p=0.022). (**g,h**) PBMC of healthy donors (n=8), ambulant patients with COVID-19 (n=6) and patients with severe COVID-19 (n=8) were stimulated with PMA/Ionomycin and the frequency (median ± SEM) of $IFN\gamma^+$ (**g**) and TNF^+ (**h**) NK cells was determined by flow cytometry. Statistical analysis was performed using the two-sided Mann-Whitney U test ($IFN\gamma^+$ NK cells ambulant *vs*. severe p=0.0007; TNF^+ NK cells ambulant *vs*. severe p=0.008). (**i**) Mean fluorescence intensity (MFI, median ± SEM) of T-bet in $CD56^{dim}$ NK cells across the disease course. Independent measurements of 53 healthy donors (n=53), 9 patients with FLI (n=9), 29 ambulant (n=62), 17 moderate (n=19) and 45 severe COVID-19 patients (n=133). For (**b-c,e-f**) and (**i**) statistical analysis was performed using a One-way ANOVA followed by a two-sided Mann-Whitney U test comparing healthy *vs*. FLI or COVID-19 groups. The dashed line indicates the median MFI or frequency of healthy donors. (*; $p \leq 0.05$, **; $p \leq 0.01$, ***; $p \leq 0.001$, ****; $p \leq 0.0001$).

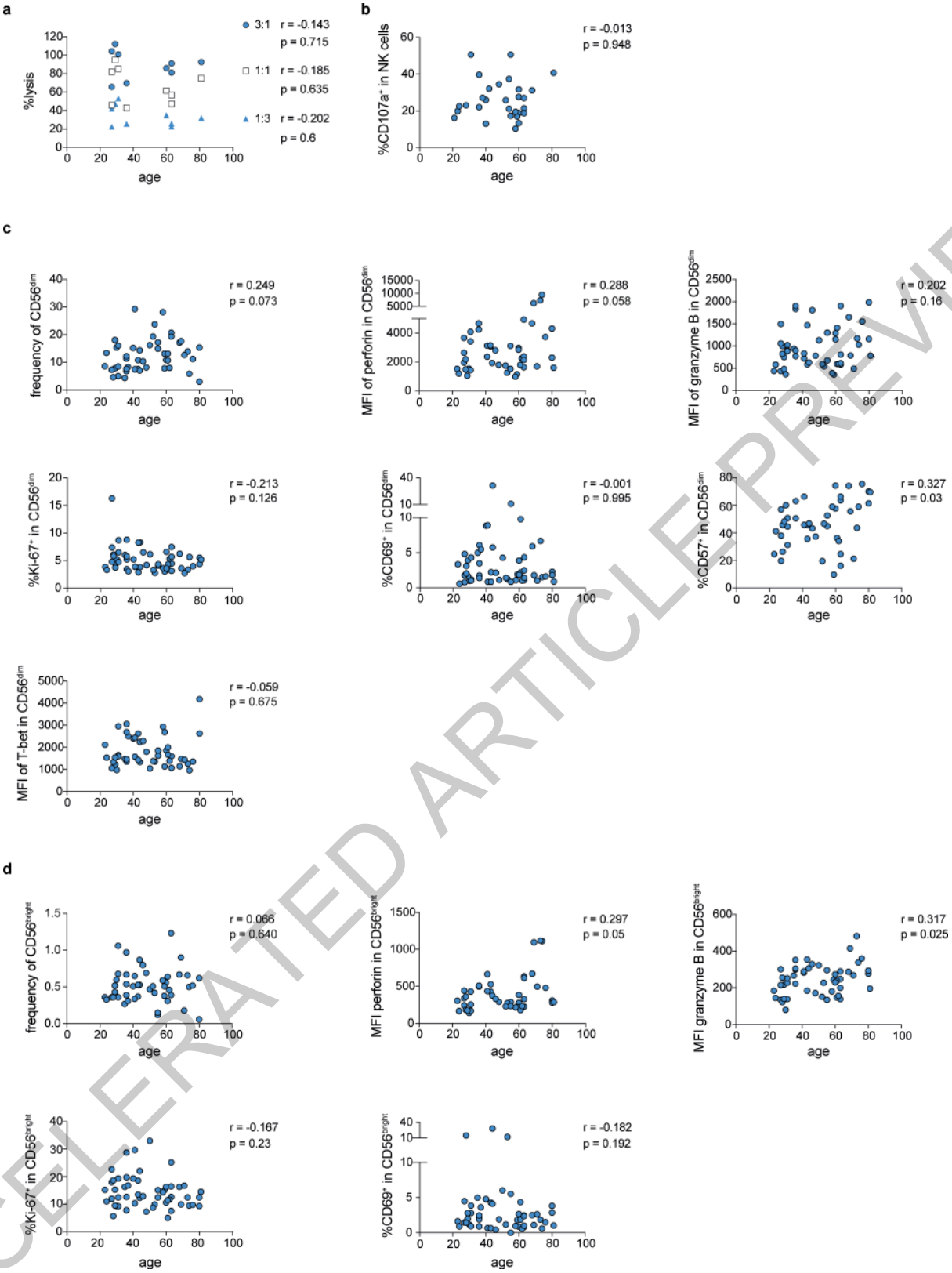

Extended Data Fig. 4 | Dysregulated NK cell function in severe COVID-19 does not correlate with age. (**a-d**) Two-tailed spearman correlation of age and ^{51}Cr release in indicated NK cell: target cell ratios in a single experiment (**a**, n=9 donors), CD107a expression in NK cells (**b**, n=29) and expression of indicated markers measured by flow cytometry in $CD56^{dim}$ (**c**) and $CD56^{bright}$ (**d**) NK cells of healthy donors (n=44 for perforin and CD57, n=50 for granzyme B, n=53 for all others). Age in years is represented by the x-axis whilst the indicated read out is represented by the y-axis.

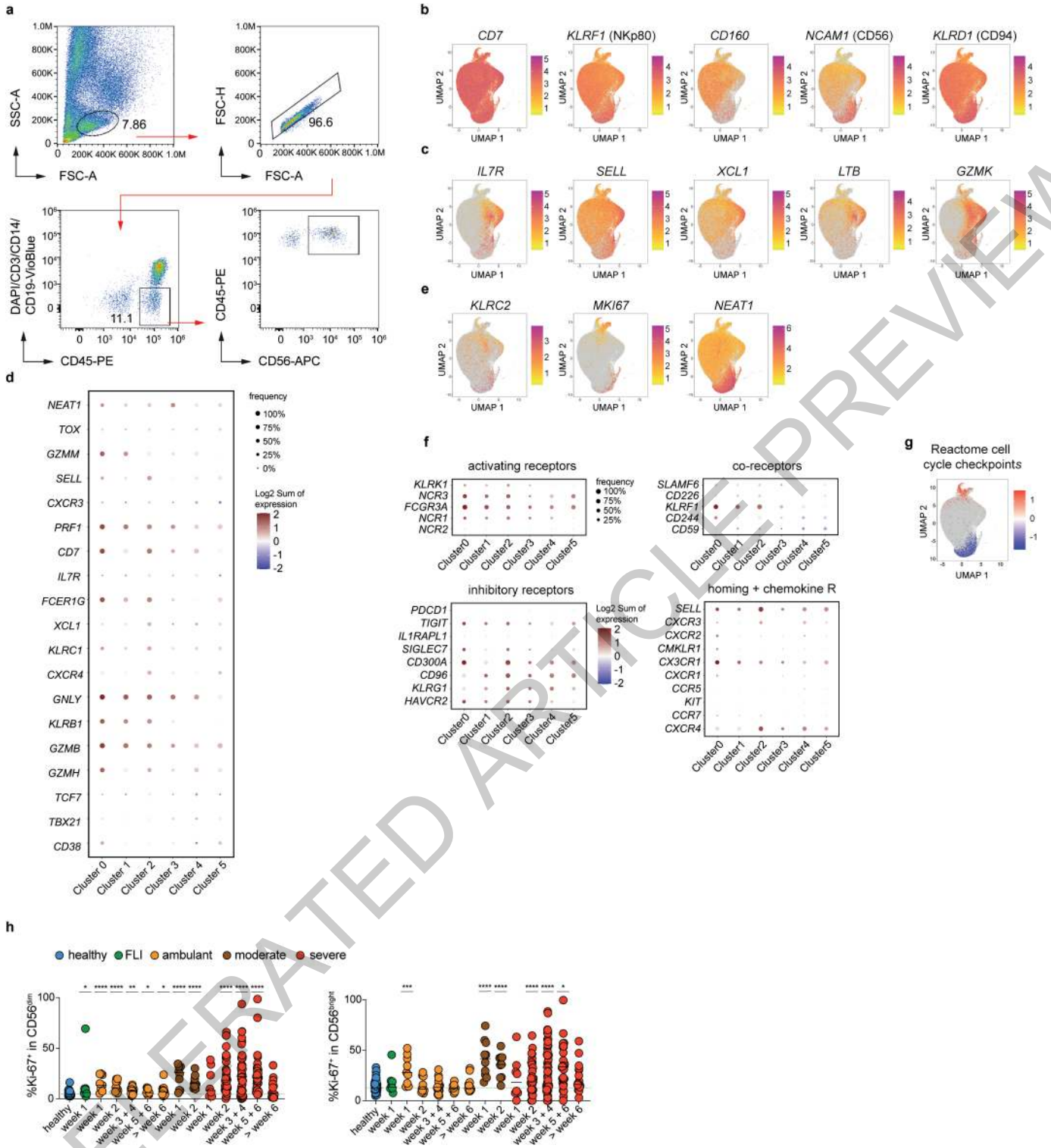

Extended Data Fig. 5 | Gene expression profile of individual NK cell clusters. (**a**) Gating strategy for FACS of peripheral blood NK cells subjected to single cell RNA sequencing. (**b,c,e**) UMAP representation depicting the expression levels of indicated genes. (**d,f**) Dot plots depicting the expression of the indicated genes in the NK cell clusters. Dot size represents the frequency of cells expressing the indicated gene. Selection of genes for each group in (**f**) according to Sivori *et al.*[55] (**g**) Single cell gene set enrichment analysis for the indicated gene set in all samples. Single cells with enriched gene expression are displayed as red dots, cells with depletion of the genes are displayed as blue dots. (**h**) Frequency of Ki-67$^+$ CD56^{dim} and CD56^{bright} NK cells (median ± SEM). Independent measurements of 53 healthy donors (n=53), 9 flu-like illness (FLI, n=9), 29 ambulant (n=62), 17 moderate (n=19) and 45 severe COVID-19 patients (n=133) between week 1 and week 11 following onset of symptoms. Statistical analysis was performed using a One-way ANOVA followed by a two-sided Mann-Whitney U test comparing healthy *vs.* FLI or COVID-19 groups. The dashed line indicates the median frequency of Ki-67$^+$ NK cells in healthy donors.

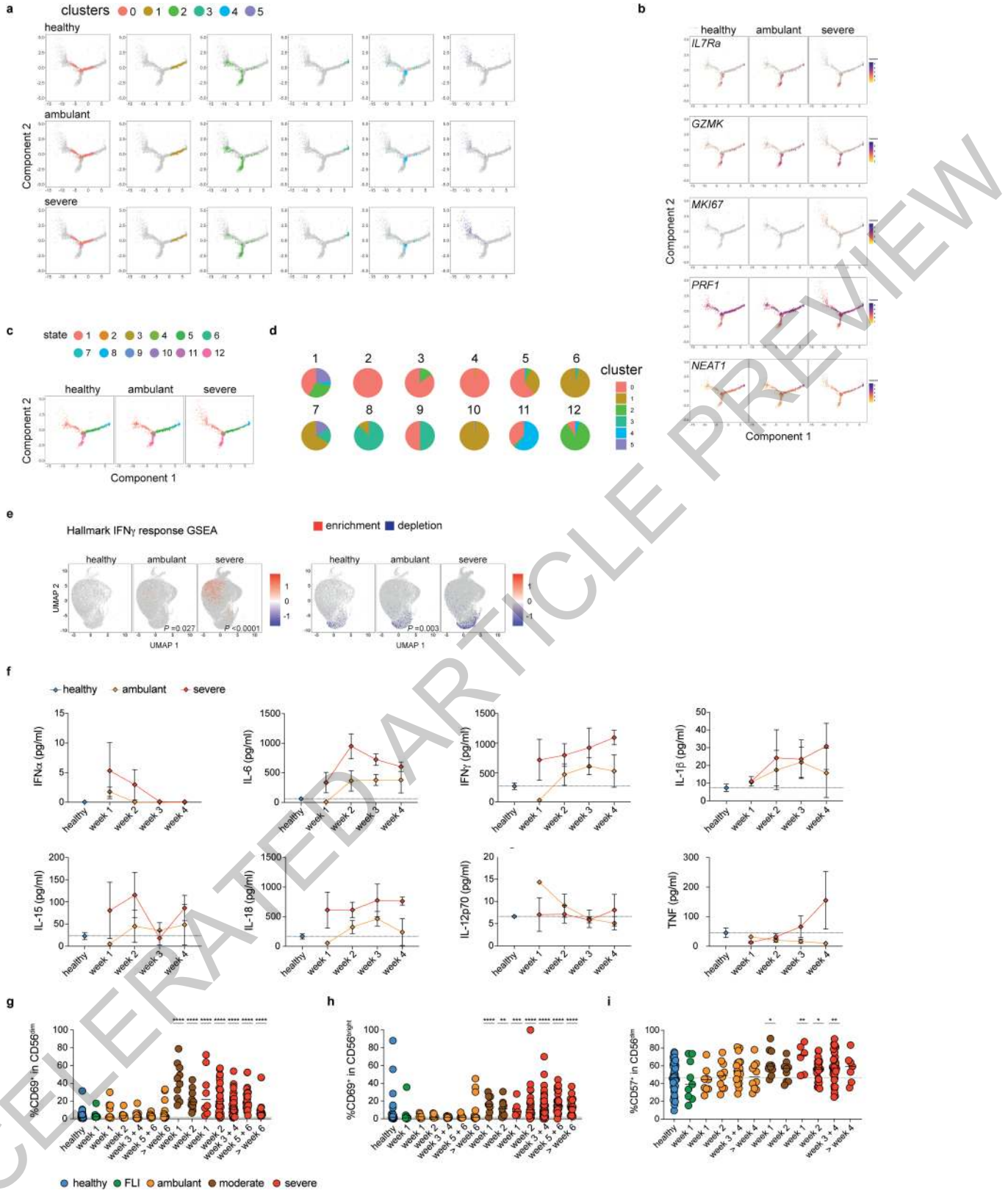

Extended Data Fig. 6 | See next page for caption.

Extended Data Fig. 6 | Differentiation trajectories of NK cells towards terminally differentiated NK cells. (**a-d**) Pseudotime trajectories of a total of 11,613 randomly selected NK cell transcriptomes from all groups. (**a**) Isolated visualization of each NK cell cluster in the pseudotime trajectory analysis. (**b**) Expression of indicated genes in the pseudotime trajectories. (**c**) Cell states in the trajectory analysis. (**d**) Pie charts depicting the representation of each NK cell cluster in the different cell states. (**e**) Single cell gene set enrichment analysis (GSEA) of the indicated gene set in the differentiated NK cell clusters (clusters 0, 1 and 3) of all samples. Single cells with enriched gene expression are displayed as red dots and cells with depletion of the genes are displayed as blue dots. Significance of the enrichment or depletion was calculated using the two-sided Fisher's exact test by comparing the indicated group with the group left-sided (ambulant *vs*. healthy and severe *vs*. ambulant, respectively). (**f**) Serum cytokine levels over the course of COVID-19. For IFNα data points represent independent measurements of 6 healthy donors (n=6), 20 ambulant patients with COVID-19 (n=27) and 17 patients with severe COVID-19 (n=26) at the indicated time points after onset of symptoms. Group size of 4 to 10 samples for COVID-19 patients per timepoint. For all other cytokines, data points represent independent measurements from 33 healthy donors (n=33), 15 ambulant patients with COVID-19 (n=20) and 6 patients with severe COVID-19 (n=17) with a group size of 3 to 8 samples for COVID-19 patients. Patients receiving corticosteroid treatment were excluded from the analysis except for the IFNα serum measurements. Bars represent the mean ± SEM. The dashed line indicates the mean serum concentration of the cytokine in healthy donors. Statistical analysis was performed using the two-sided Mann-Whitney U test. (**g,h**) Frequency (median ± SEM) of $CD69^{+}$ $CD56^{dim}$ (**g**) and $CD56^{bright}$ NK cells (**h**). Independent measurements of 53 healthy donors (n=53), 9 flu-like illness (FLI, n=9), 29 ambulant (n=62), 17 moderate (n=19) and 45 severe COVID-19 patients (n=133) between week 1 and week 11 after onset of symptoms. (**i**) Quantification of $CD57^{+}$ $CD56^{dim}$ NK cells (median ± SEM). Independent measurements from 44 (n=44) healthy donors, 9 patients with FLI (n=9), 24 ambulant (n=56), 17 moderate (n=19) and 30 severe COVID-19 patients (n=73) from week 1 to 8 after onset of symptoms. Statistical analysis in **c-e** was performed using a One-way ANOVA followed by a two-sided Mann-Whitney U test comparing healthy *vs*. FLI or COVID-19 groups. The dashed line indicates the median frequency in healthy donors.

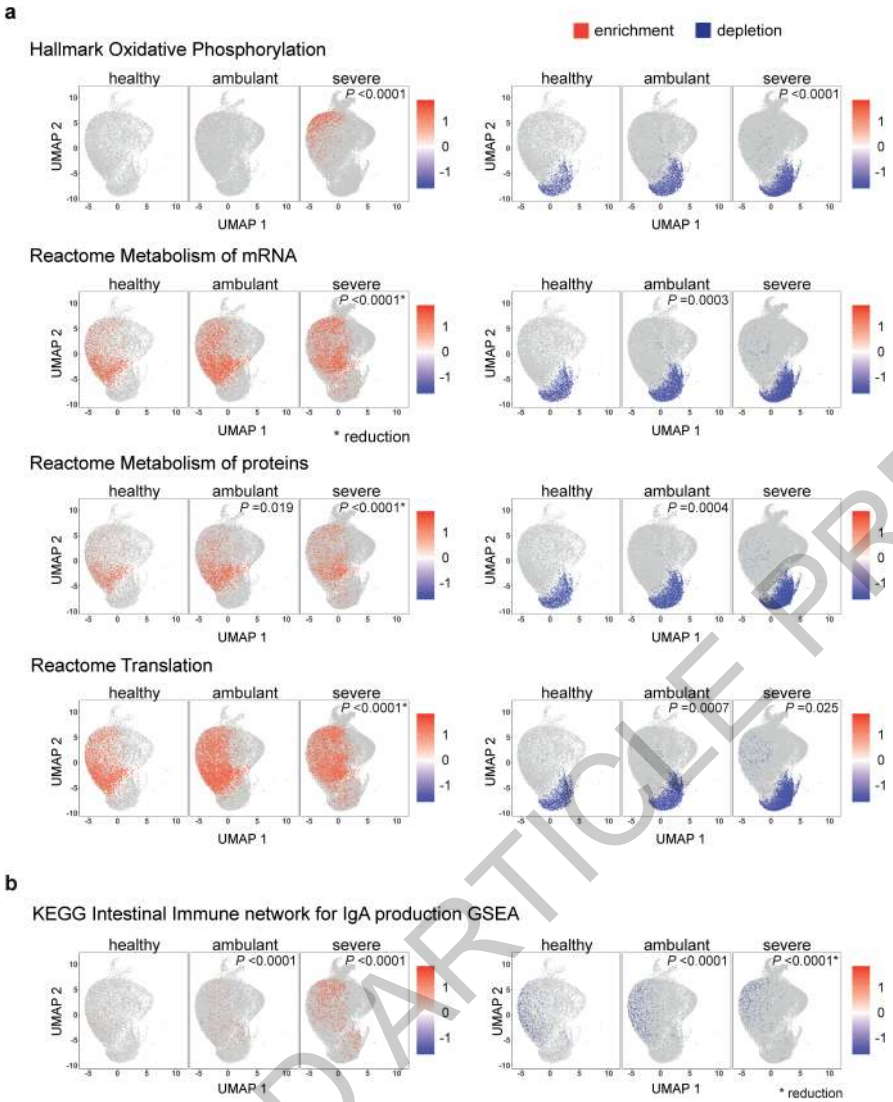

Extended Data Fig. 7 | NK cells show profound changes in gene networks related to cellular metabolism and intestinal IgA production during COVID-19. (**a**,**b**) Single cell gene set enrichment analysis (GSEA) of the indicated gene sets in the differentiated NK cell clusters (clusters 0, 1 and 3) of all samples. Single cells with enriched gene expression are displayed as red dots and cells with depletion of the genes are displayed as blue dots. Significance of the enrichment or depletion was calculated using the two-sided Fisher's exact test by comparing the indicated group with the group left-sided (ambulant *vs.* healthy and severe *vs.* ambulant, respectively). P-value* describes a reduction in enrichment or depletion.

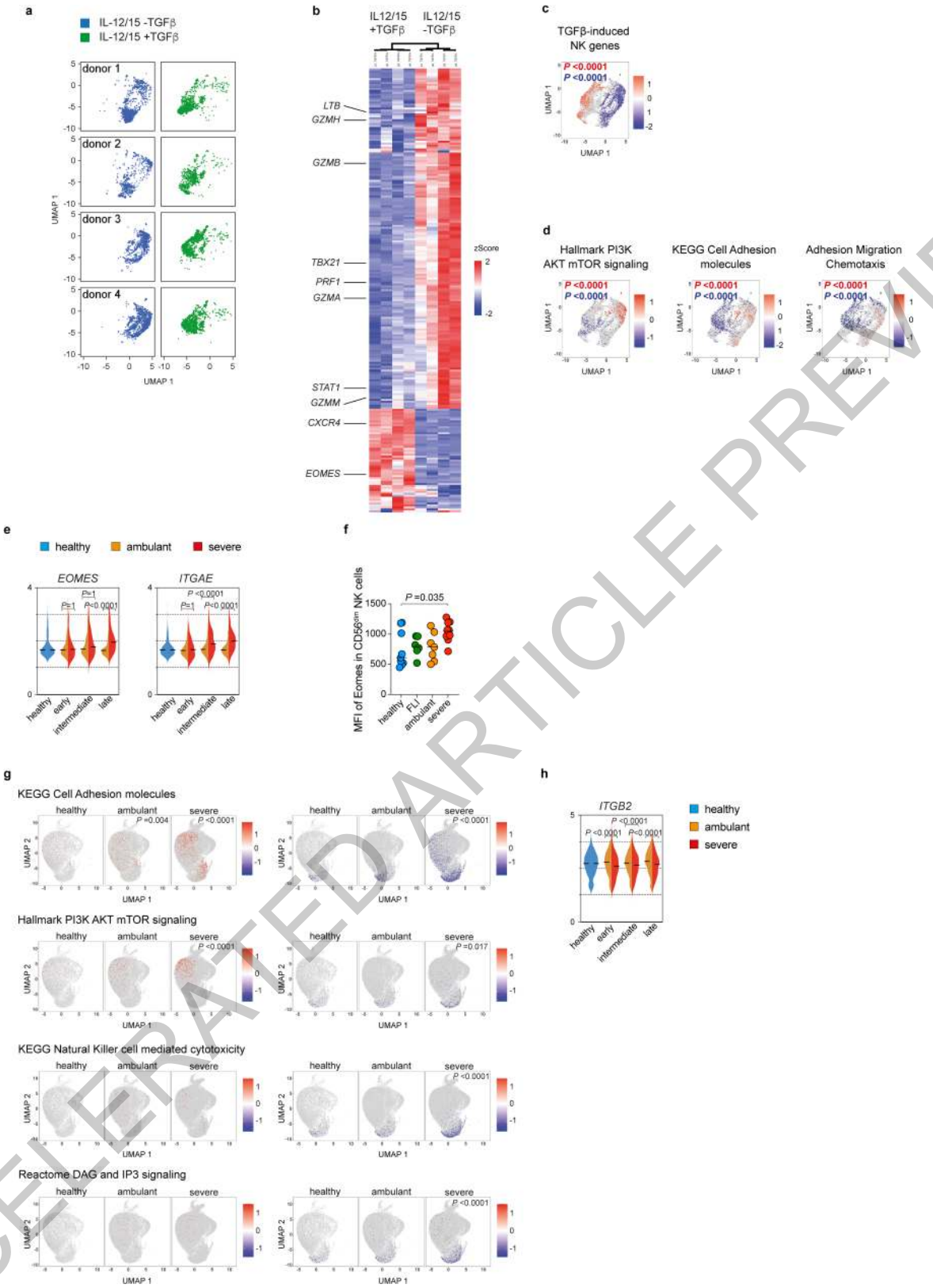

Extended Data Fig. 8 | See next page for caption.

Extended Data Fig. 8 | Genes related to cell adhesion are suppressed in NK cells during severe COVID-19 and by *in vitro* exposure to TGFβ. (**a,b**) Peripheral blood NK cells of 4 healthy donors were FACS-sorted and cultured *in vitro* in the presence of either IL-12, IL-15 and TGFβ or IL-12 and IL-15 alone and a total of 8137 single cell transcriptomes were generated. (**a**) UMAP representation of single cell transcriptomes of the four donors for both conditions. (**b**) Heatmap shows differentially expressed genes between both conditions. Upregulated genes are displayed in red, downregulated genes in blue. (**c,d**) Single cell GSEA of the NK cell-specific TGFβ response gene data set (**c**) or the indicated gene sets (**d**) projected on the UMAP of the scRNA-seq data obtained from NK cells cultured *in vitro* in the presence or absence of TGFβ as described above. Red dots represent cells with increased expression of the indicated gene set. Blue dots represent cells with a depletion of genes within the indicated gene set. Significance of the enrichment or depletion was calculated using the two-sided Fisher's exact test. (**e,h**) Violin Plot showing the median expression of the indicated genes in differentiated NK cell clusters (0,1 and 3) of healthy individuals and in ambulant and severe COVID-19 patients during the course of disease (Early: <day 14 after symptom onset, intermediate: day 15-28, late: > day 28, two-sided Mann-Whitney U test, p-value adjusted for multiple comparisons). (**f**) MFI of Eomes was measured in $CD56^{dim}$ NK cells from 9 healthy donors (n=9 independent measurements), 6 patients with FLI (n=6), 7 ambulant (n=7) and 9 severe COVID-19 (n=10). Statistical analysis was performed using a One-way ANOVA followed by a two-sided Mann-Whitney U test comparing healthy *vs*. FLI or COVID-19 groups. (**g**) Single cell gene set enrichment analysis (GSEA) of the indicated gene sets in the differentiated NK cell clusters (clusters 0, 1 and 3) of all samples. Single cells with enriched gene expression are displayed as red dots and cells with depletion of the genes are displayed as blue dots. Significance of the enrichment or depletion was calculated using the two-sided Fisher's exact test by comparing the indicated group with the group left-sided (ambulant *vs*. healthy and severe *vs*. ambulant, respectively).

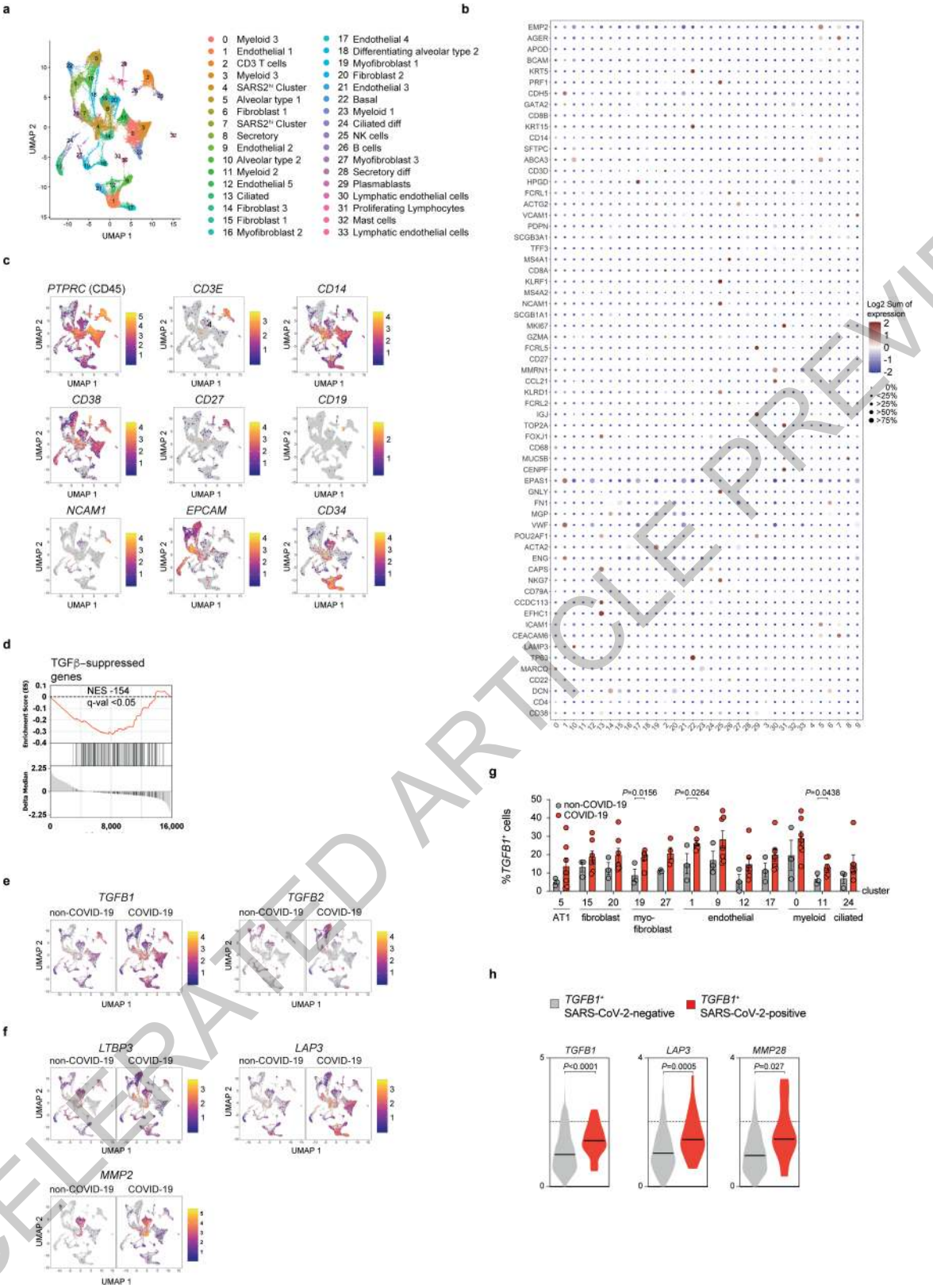

Extended Data Fig. 9 | See next page for caption.

Extended Data Fig. 9 | TGFβ expression is induced in lung tissue hematopoietic and non-hematopoietic cell populations during COVID-19. (**a-h**) Single-nucleus sequencing of lung tissue from patients with SARS-CoV-2-negative pneumonia (non-COVID-19) and severe COVID-19[31]. (**a**) UMAP visualization of single-nucleus transcriptomes (>52,000) and identification of cellular populations according to (ref. [31]). (**b**) Dot plot depicting the expression of the indicated genes in the various clusters. Dot size represents the frequency of cells expressing the indicated gene. (**c**) UMAPs showing the expression of the indicated genes in all cells. (**d**) GSEA of TGFβ-suppressed NK cells genes in lung tissue-resident NK cells extracted from the data set. (**e,f**) UMAP representation of indicated genes in all cells of non-COVID-19 and COVID-19 patients. (**g**) Quantification of the frequency of *TGFB1*$^+$ cells per cluster per patient in both groups. Only clusters represented by cells were included. Bars display mean ± SEM (non-COVID-19: all n=3 patients, COVID-19: cluster 24; n=6, cluster 27; n=4, all other clusters n=7, p-value was determined by two-sided t-test). (**h**) Expression level of indicated genes in *TGFB1*$^+$ SARS-CoV-2-negative cells and *TGFB1*$^+$ SARS-CoV-2-positive cells of all COVID-19 samples. Significance was calculated using the two-sided Mann-Whitney U-Test.

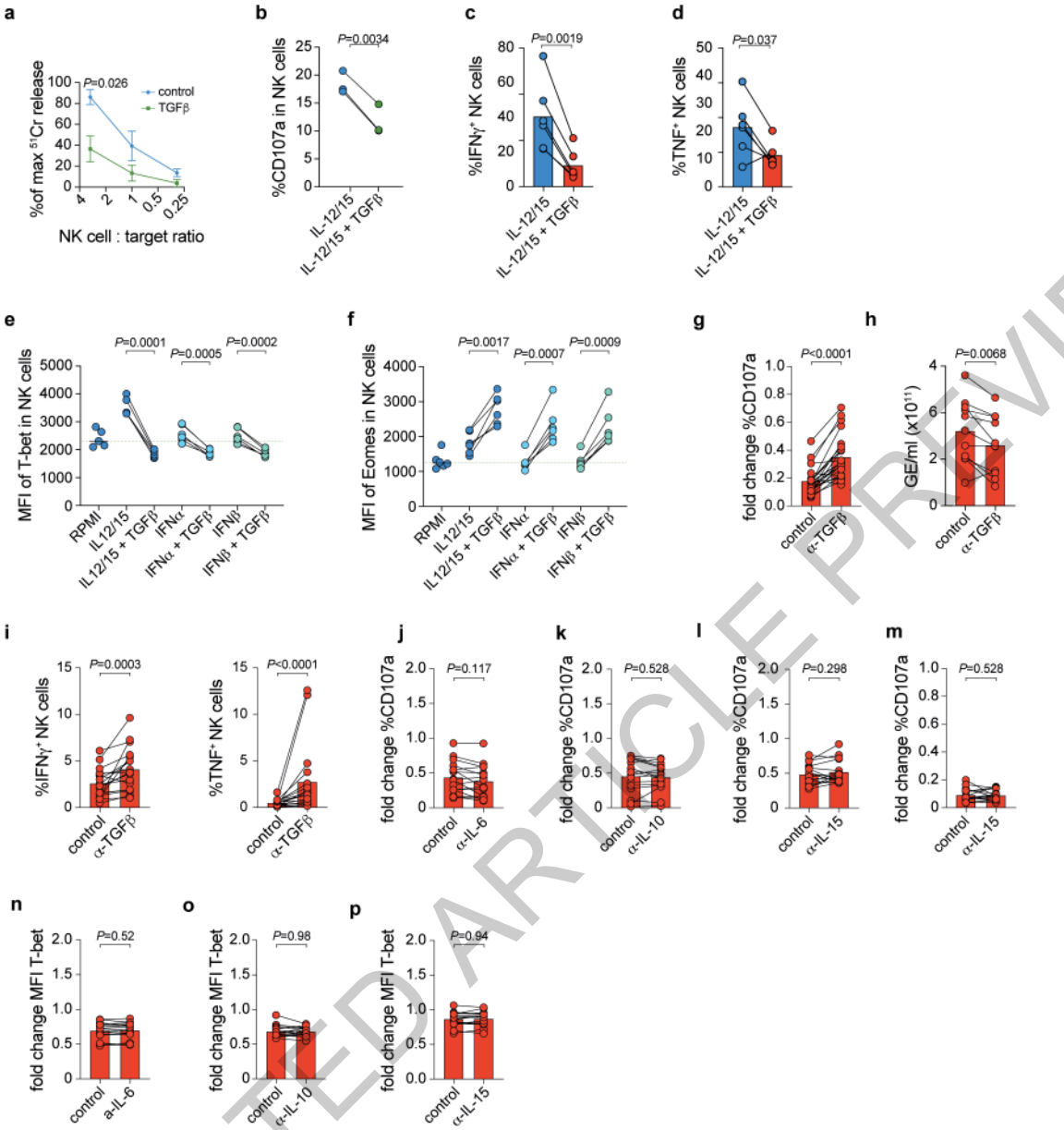

Extended Data Fig. 10 | Serum from severe COVID-19 patients suppresses NK cells in a TGFβ-dependent manner. (**a**) NK cells were cultured in medium with (green) or without TGFβ (blue). Specific lysis (mean ± SEM; n=3 healthy donors) of K562 target cells was determined in a ^{51}Chromium release assay. Significance determined by two-sided unpaired t-test. (**b**) Sorted NK cells of healthy donors were cultured in medium containing the indicated cytokines with and without TGFβ. The frequency of CD107a$^+$ NK cells was analyzed after 4h co-culture with K562 cells (n=3 per group). **(c,d)** PBMC of healthy donors (n=6) were cultured for 4 days with the indicated cytokines and the frequency of IFNγ$^+$ (**c**) and TNF$^+$ NK cells (**d**) was determined after PMA/Iono stimulation. (**e,f**) Sorted NK cells of healthy donors were cultured for 4 days in medium containing the indicated cytokines. The MFI of T-bet (**e**) and Eomes (**f**) was measured by flow cytometry. The dashed line indicates median MFI of NK cells cultured in medium only (RPMI and IL-12/15 in **e** n=5 donors, all others n=6). (**g-p**) Sorted NK cells from 3 to 4 healthy donors per experiment were cultured in medium containing the cytokines IL-2 and IL-12 (**g,m**), IL-12 and IL-15 (**h-k, n-o**) or IL-2 (**l,p**) either alone or with serum from 3 to 6 patients with severe COVID-19 per experiment. In a second condition, patient sera were pre-incubated as indicated with anti-TGFβ, anti-IL-6, anti-IL-10 or anti-IL-15 antibody before adding to the culture. The frequency of CD107a$^+$ NK cells (**g,j-m**), the frequency of IFNγ$^+$/TNF$^+$ NK cells after 4h co-culture with K562 cells (**i**), the viral load after co-culture with SARS-CoV-2-infected Vero E6 cells (**h**) and the MFI of T-bet (**n-p**) was determined. Fold change frequency or MFI was calculated between NK cells cultured in patients' sera (+/- prior anti-TGFβ treatment) and NK cells cultured in medium only. Each dot represents NK cells from one healthy donor cultured with severe COVID-19 serum (+/- prior anti-TGFβ treatment) (**g**; n=24, **i**; n=18, **j-p**; n=16, **h**; n=11 pooled samples derived from 3 patients, NK:target cell ratio 1:3, 1:1, 3:1, 9:1). Statistical analysis was performed using two-sided paired t-test (**b-f**) or two-sided Wilcoxon matched-pairs rank test (**g-p**).

nature research

Corresponding author(s): Andreas Diefenbach
Mario Witkowski

Last updated by author(s): Sep 29, 2021

Reporting Summary

Nature Research wishes to improve the reproducibility of the work that we publish. This form provides structure for consistency and transparency in reporting. For further information on Nature Research policies, see our Editorial Policies and the Editorial Policy Checklist.

Statistics

For all statistical analyses, confirm that the following items are present in the figure legend, table legend, main text, or Methods section.

n/a	Confirmed	
☐	☒	The exact sample size (*n*) for each experimental group/condition, given as a discrete number and unit of measurement
☐	☒	A statement on whether measurements were taken from distinct samples or whether the same sample was measured repeatedly
☐	☒	The statistical test(s) used AND whether they are one- or two-sided *Only common tests should be described solely by name; describe more complex techniques in the Methods section.*
☒	☐	A description of all covariates tested
☐	☒	A description of any assumptions or corrections, such as tests of normality and adjustment for multiple comparisons
☐	☒	A full description of the statistical parameters including central tendency (e.g. means) or other basic estimates (e.g. regression coefficient) AND variation (e.g. standard deviation) or associated estimates of uncertainty (e.g. confidence intervals)
☒	☐	For null hypothesis testing, the test statistic (e.g. *F*, *t*, *r*) with confidence intervals, effect sizes, degrees of freedom and *P* value noted *Give P values as exact values whenever suitable.*
☒	☐	For Bayesian analysis, information on the choice of priors and Markov chain Monte Carlo settings
☒	☐	For hierarchical and complex designs, identification of the appropriate level for tests and full reporting of outcomes
☐	☒	Estimates of effect sizes (e.g. Cohen's *d*, Pearson's *r*), indicating how they were calculated

Our web collection on statistics for biologists contains articles on many of the points above.

Software and code

Policy information about availability of computer code

Data collection	Cell sorting for single cell sequencing was performed using a MA900 Multi-Application Cell Sorter (Sony Biotechnology). For in vitro cultures NK cells were sorted using a FACS Aria II Cell Sorter (BD Biosciences). Flow cytometry data was acquired using FACS Fortessa X20 (BD Biosciences).
Data analysis	Flow cytometry data was analyzed using FlowJo Software V10.3 (Treestar). Statistical analysis was performed using GraphPad - Prism (version 8).

For manuscripts utilizing custom algorithms or software that are central to the research but not yet described in published literature, software must be made available to editors and reviewers. We strongly encourage code deposition in a community repository (e.g. GitHub). See the Nature Research guidelines for submitting code & software for further information.

Data

Policy information about availability of data

All manuscripts must include a data availability statement. This statement should provide the following information, where applicable:

- Accession codes, unique identifiers, or web links for publicly available datasets
- A list of figures that have associated raw data
- A description of any restrictions on data availability

Data used for this study will be available in Gene Expression Omnibus (GEO) before publication.

Field-specific reporting

Please select the one below that is the best fit for your research. If you are not sure, read the appropriate sections before making your selection.

☒ Life sciences ☐ Behavioural & social sciences ☐ Ecological, evolutionary & environmental sciences

For a reference copy of the document with all sections, see nature.com/documents/nr-reporting-summary-flat.pdf

Life sciences study design

All studies must disclose on these points even when the disclosure is negative.

Sample size	Sample size was determined by the availability of patient material at the time of study
Data exclusions	For selected analyses samples from patients receiving corticosteroids were excluded as indicated.
Replication	Each biological sample was analyzed independently (group sizes as indicated). For chromium release assays triplicates were used for each biological sample.
Randomization	Not applicable as each patient sample (healthy controls, Flu-like illness, ambulant COVID-19/moderate COVID-19/severe COVID-19) was analyzed indepently upon collection according to sample availability at the time of analysis.
Blinding	Blinding was not possible due to the nature of the samples analyzed. Patient samples (healthy controls, Flu-like illness, ambulant COVID-19, moderate COVID-19, severe COVID-19) were obtained from different health care areas (outpatient clinic, regular ward, intensive care unit, healthy controls outside of health care context).

Reporting for specific materials, systems and methods

We require information from authors about some types of materials, experimental systems and methods used in many studies. Here, indicate whether each material, system or method listed is relevant to your study. If you are not sure if a list item applies to your research, read the appropriate section before selecting a response.

Materials & experimental systems

n/a	Involved in the study
☐	☒ Antibodies
☐	☒ Eukaryotic cell lines
☒	☐ Palaeontology and archaeology
☒	☐ Animals and other organisms
☐	☒ Human research participants
☒	☐ Clinical data
☒	☐ Dual use research of concern

Methods

n/a	Involved in the study
☒	☐ ChIP-seq
☐	☒ Flow cytometry
☒	☐ MRI-based neuroimaging

Antibodies

Antibodies used

Anti-human antibodies:

Flow Cytometry:
CD3 (BW264/56, VioBlue, Miltenyi Biotec, Cat No 130-113-133)
CD14 (TÜK4, VioBlue, Miltenyi Biotec, Cat No 130-113-152)
CD19 (LT19, VioBlue, Miltenyi Biotec, Cat No 130-113-172)
CD57 (TBO1, eF450, ThermoFisher, Cat No 48-0577-42)
Cell Proliferation Dye (VioBlue, ThermoFisher, Cat No 65-0842-85)
CD127 (A019D5, BV421, BioLegend, Cat No 351309)
NKp30 (p30-15, BV421, BD Bioscience, Cat No 563385)
Zombie Aqua Fixable Viability Kit (V500, BioLegend, Cat No 423101)
T-bet (4B10, BV605, BioLegend, Cat No 644817)
CD161 (HP-3G10, BV785, BioLegend, Cat No 339930)
Ki-67 (B56, PerCP-Cy5.5, BD Biosciences, Cat No 561284)
CD226 (11A8, PerCP-Cy5.5, BioLegend, Cat No 338314)
CD45 (QA17A19, PerCP/Cyanine5.5, BioLegend, Cat No 393409)
Granzyme B (GB11, PE, ThermoFisher, Cat No 12-8899-41)
TNF (Mab11, PE, BioLegend, Cat No 502908)
CD45 (HI30, PE, BioLegend, Cat No 304008)
CD117 (104D2, PE, BioLegend, Cat No 983304)
CD7 (CD7-6B7, PE/Dazzle, BioLegend, Cat No 343119)

CD69 (FN50, PE-Cy7, BD Bioscience, Cat No 557745)
IFNγ (4S.B3, PE-Cy7, BioLegend, Cat No 502527)
NKp44 (2.29, PE-Cy7, Miltenyi Biotec, Cat No 130-120-487)
Eomes (WD1928, PE-Cy7, ThermoFisher, Cat No 25-4877-42)
Perforin (dG9, APC, ThermoFisher, Cat No 17-9994-42)
CD107a (H4A3, APC, BD Bioscience, Cat No 562622)
CD56 (AF12-7H3, APC, Miltenyi Biotec, Cat No 130-113-305)
CD8 (SFCI21, APC, Beckman Coulter, Cat No IM2469)
CD294 (BM16, APC, BioLegend, Cat No 350103)
NKp46 (9E2, APC, Miltenyi Biotec, Cat No 130-092-609)
CellTrace (APC, ThermoFisher, Cat No C34564)
CD56 (5.1H11, APC/Cyanine7, BioLegend, Cat No 362511)
CD3 (UCH-T1, APC-750, Beckman Coulter, Cat No A94680)
CD16 (3G8, BUV395, BD Bioscience, Cat No 563785)
CD3 (HIT3a, FITC, ThermoFisher, Cat No 11-0039-42)
CD4 (OKT4, FITC, ThermoFisher, Cat No 11-0048-42)
CD14 (HCD14, FITC, BioLegend, Cat No 325604)
CD19 (SJ25C1, FITC, BioLegend, Cat No 363008)
CD107a (eBioA4H3, FITC, eBioscience, Cat No 11-1079-42)
CD56 (N901, ECD, Beckman Coulter, Cat No A82943)
CD45 (J33, KrO, Beckman Coulter, Cat No B36294)

Validation

All purchased antibodies were validated by their manufacturers and further in-house testing.
- Miltenyi Biotec, https://www.miltenyibiotec.com/DE-en/lp/antibody-validation-improved-reproducibility.html
Three pillars of antibody validation: 1. Antibody reproducibility and consistency (Pure antibody products & Lot-to-lot consistent performance); 2. Antibody specificity (Epitope competition assay,Knockout validation via targeted genome editing & RNAi knockdown); 3. Antibody sensitivity (Functional testing of every product prior to release, Performance comparison & Compatibility with fixation).

- BioLegend, https://www.biolegend.com/en-us/reproducibility
The reproducibility of published research has emerged as an urgent topic in today's scientific community. From funding agencies to researchers to manufacturers and publishers, it is critical for all of these groups to align themselves to ensure that research is done with rigor and is reproducible. How has BioLegend stepped up to meet these needs? In addition to sponsoring and collaborating with the Global Biological Standards Institute (GBSI) on setting antibody standards, we undertake extensive measures to ensure quality products that meet reproducibility requirements today and into the future.
BioLegend spends a considerable amount of effort in creating new antibodies for research. The majority of these new antibody products are monoclonal antibodies (mAb) produced from hybridomas. Clones of these hybridomas are carefully selected based on a number of criteria including robust growth and efficient production of a single clone of antibody that is specific to the intended target. The best clones move on to applications testing. All newly developed clones at BioLegend undergo validation testing for multiple applications. This serves as a cross-check for specificity and provides clarity for research uses. Maintaining lot-to-lot consistency is vital for reproducibility. It simply is not enough for antibody manufacturers to validate antibodies just once. Pass/fail specification requirements are essential for quality control testing of every lot of product. BioLegend maintains records for all lotspecific testing
- BD Biosciences, https://www.biocompare.com/Antibody-Manufacturing/355107-Antibody-Manufacturing-Perspectives-BDBioscience/
We conduct quality control (QC) testing in primary model systems to ensure biological accuracy in an ISO 9001 certified facility. BD carefully selects and characterizes antibody content in product development and tests in relevant primary model systems to ensure biological accuracy. BD conducts rigorous QC testing of each antibody lot tested side-by-side with a previously produced lot as reference. Our product development process includes testing on a combination of primary cells, cell lines and/or transfectant cell models with relevant controls using multiple immunoassays to ensure biological accuracy. We also perform multiplexing with additional antibodies to interrogate antibody staining in multiple cell populations. BD believes antibody validation is critical to ensure accurate scientific results. Both the consumer and the reagent provider share the responsibility for reproducible science.

- Invitrogen, https://www.thermofisher.com/de/de/home/life-science/antibodies/invitrogen-antibody-validation.html
Antibodies are some of the most critical research reagents used in the lab. Poor specificity or application performance can significantly frustrate the ability to obtain good results, which can cause critical delays. Underperforming antibodies result in a lack of reproducibility, wasting time and money. In other words, researchers need antibodies that bind to the right target and work in their applications every time. To help ensure superior antibody results, we've expanded our specificity testing methodology using a 2-part approach for advanced verification. Part 1—Target specificity verification. This helps ensure the antibody will bind to the correct target. Our antibodies are being tested using at least 1 of the following methods to ensure proper functionality in researcher's experiments. Part 2—Functional application validation. These tests help ensure the antibody works in a particular application(s) of interest.

- Beckman Coulter, https://www.beckman.de/reagents/coulter-flow-cytometry/antibodies-and-kits/single-color-antibodies/quality-standards
Development and production of our conjugated antibodies under current Good Manufacturing Practices (cGMP) in facilities that adhere and are certified to the highest standards in the industry.
Having more than 30 years of experience in conjugated antibody development and manufacturing, associated with the strictest internal quality controls that demonstrate lot-to-lot consistency over time in all our products.

Eukaryotic cell lines

Policy information about cell lines

Cell line source(s)

K562 (ATCC-10), Vero E6 (ATCC® CRL-1586™), Calu-3 (ATCC® HTB-55™)

Authentication	From vendor. ATCC authenticates cell lines routinely by STR profiling, cellular morphology, karyotyping and cytochrome C oxidase I assay.
Mycoplasma contamination	Cells were not tested for mycoplasma contamination during the time of the study. Cell line viability ≥ 90% was confirmed prior co-culture.
Commonly misidentified lines (See ICLAC register)	No commonly misidentified lines were used in this study.

Human research participants

Policy information about studies involving human research participants

Population characteristics	45 ambulant patients with COVID-19 (WHO 1 and 2 according to the WHO clinical ordinal scale) and 21 hospitalized patients with moderate COVID-19 (WHO2-4), 79 hospitalized patients with severe COVID-19 requiring ventilation (WHO 5-7) were enrolled in this study. All COVID-19 patients were tested positive for SARS-CoV-2 RNA via nasopharyngeal swabs. 20 patients presenting flu-like symptoms but were tested negative for SARS-CoV-2 (Flu-like illness, FLI) and a total of 96 healthy donors who did not present any clinical sign of viral infection were enrolled as controls (seronegative for SARS-CoV-2-specific antibodies).
Recruitment	All hospitalized patients were recruited from the regular ward or the Intensive Care Unit of the Charité. SARS-CoV-2 infection was verified by SARS-CoV-2 RNA via nasopharyngeal swabs. Ambulant COVID-19 patients (SARS-CoV-2 infection verified by SARS-CoV-2 RNA via nasopharyngeal swabs) and patients with Flu-like illness (negative for SARS-CoV-2 RNA via nasopharyngeal swabs) were recruited from the outpatient clinics in Berlin. 96 healthy donors who did not present any clinical sign of viral infection were enrolled as controls (negative for SARS-CoV-2-specific antibodies), recruitment in the Charité (health care workers) and in outpatient clinics.
Ethics oversight	Institutional Review Board of the Charité (EA2/066/20, EA2/072/20, EA4/014/20 and EA2/092/20)

Note that full information on the approval of the study protocol must also be provided in the manuscript.

Flow Cytometry

Plots

Confirm that:

☒ The axis labels state the marker and fluorochrome used (e.g. CD4-FITC).

☒ The axis scales are clearly visible. Include numbers along axes only for bottom left plot of group (a 'group' is an analysis of identical markers).

☐ All plots are contour plots with outliers or pseudocolor plots.

☒ A numerical value for number of cells or percentage (with statistics) is provided.

Methodology

Sample preparation	Peripheral blood mononuclear cells (PBMC) were separated from peripheral blood by Pancoll human (PAN-Biotech) density gradient centrifugation at room temperature (RT). Cells were either used directly for analysis or stored in heat-inactivated fetal bovine serum (FCS, Pan- Biotech Cat# P30-3602) with 10% DMSO at -80°C prior to analysis. PBMC were incubated with Fc Blocking Reagent (Miltenyi Biotec) according to manufacturer's instructions. To exclude dead cells, the cells were stained with a LIVE/DEAD (LD) Fixable Aqua Dead Cell staining Kit (ThermoFisher, Cat# L34965). For surface antigen staining the cells were incubated with monoclonal anti-human antibodies for 20min at 4°C. The Foxp3 Transcription Factor Staining Buffer Set (eBioscience, Cat# 00-5523-00) was applied prior to intracellular staining of transcription factors, cytotoxic molecules and cytokines.
Instrument	The samples were analyzed using FACS Fortessa X20 (BD Biosciences) for flow cytometry analysis. Cell sorting for single cell sequencing was performed using a MA900 Multi-Application Cell Sorter (Sony Biotechnology). For in vitro cultures NK cells were sorted using a FACS Aria II Cell Sorter (BD Biosciences).
Software	Data was analyzed using FlowJo Software V10.3 (Treestar).
Cell population abundance	Cell population abundance was highly variable among patient groups and healthy controls. Purity of the sorted cell population was analyzed in a post-sort reanalysis. Cell counting for single cell sequencing was performed using a MACSQuant flow cytometer (Miltenyi Biotec).
Gating strategy	NK cells were sorted as DAPI- CD3- CD14- CD19- CD45+ CD56+ (for sequencing) or CD3- CD14- CD19- CD4- CD45+ CD7+ CD56 + (for in vitro experiments. Gating strategy for individual phenotyping experiments as indicated in the manuscript.

☒ Tick this box to confirm that a figure exemplifying the gating strategy is provided in the Supplementary Information.